



Benefits of simulating precipitation characteristics over Africa with a regionally-coupled atmosphere–ocean model

Torsten Weber¹ · William Cabos² · Dmitry V. Sein^{3,4} · Daniela Jacob¹

Received: 14 September 2021 / Accepted: 2 May 2022
© The Author(s) 2022

Abstract

High-quality climate information at appropriate spatial and temporal resolution is essential to develop and provide tailored climate services for Africa. A common method to produce regional climate change data is to dynamically downscale global climate projections by means of regional climate models (RCMs). Deficiencies in the representation of the sea surface temperatures (SSTs) in earth system models (ESMs) and missing atmosphere–ocean interactions in RCMs contribute to the precipitation bias. This study analyzes the influence of the regional atmosphere–ocean coupling on simulated precipitation and its characteristics over Africa, and identifies those regions providing an added value using the regionally coupled atmosphere–ocean model ROM. For the analysis, the MPI-ESM-LR historical simulation and emission scenario RCP8.5 were dynamically downscaled with ROM at a spatial resolution of $0.22^\circ \times 0.22^\circ$ for the whole African continent, including the tropical Atlantic and the Southwest Indian Ocean. The results show that reduced SST warm biases in both oceans lead to more realistic simulated precipitation over most coastal regions of Sub-Saharan Africa and over southern Africa to varying degrees depending on the season. In particular, the annual precipitation cycles over the coastal regions of the Atlantic Ocean are closer to observations. Moreover, total precipitation and extreme precipitation indices in the coupled historical simulation are significantly lower and more realistic compared to observations over the majority of the analyzed sub-regions. Finally, atmosphere–ocean coupling can amplify or attenuate climate change signals from precipitation indices or even change their sign in a regional climate projection.

Keywords Regional climate modelling · Atmosphere–ocean coupling · Sea surface temperature bias · Regional climate change · Precipitation characteristics · Africa

1 Introduction

Realistically simulated precipitation and derived precipitation indices are key elements for tailored climate change information. Based on this knowledge, climate adaptation strategies and measures can be developed to prevent or decrease potential negative impacts of climate change. This

kind of information and actions are particularly needed for Africa, as it is one of the continents most affected by climate change (Niang et al. 2014).

Several investigations were conducted to analyze possible future precipitation changes over Africa using ensembles of regional climate projections (Nikulin et al. 2018; Weber et al. 2018b; Dosio et al. 2019). To generate such projections, regional climate models (RCMs) have been applied to dynamically downscale global climate projections from earth system models (ESMs) using their simulated sea surface temperatures (SSTs) and their atmospheric fields as boundary conditions. However, it has already been shown that most ESMs have deficiencies in simulating the SST of the Benguela upwelling area offshore the African coast in the Southeast Atlantic Ocean, which lead to a warm SST bias (e.g. Toniazzo and Woolnough 2014; Xu et al. 2014; Găinușă-Bogdan et al. 2018). The processes responsible for the warm SST bias in the Southeast Atlantic in ESMs vary

✉ Torsten Weber
torsten.weber@hereon.de

¹ Climate Service Center Germany (GERICS),
Helmholtz-Zentrum Hereon, Hamburg, Germany

² Departamento de Física Y Matemáticas, Universidad de
Alcalá, Alcalá de Henares, Madrid, Spain

³ Alfred Wegener Institute for Polar and Marine Research,
Bremerhaven, Germany

⁴ Shirshov Institute of Oceanology, Russian Academy
of Science, Moscow, Russia

from model to model. For instance, Exarchou et al. (2018) found that there is a too strong absorption in the ocean mixed layer, which can be associated with a too excessive insulation caused by unrealistically low clouds, and a missing spatial and temporal variability of the biological productivity in the ocean. They also showed that the warm SST bias is related to insufficient turbulent vertical mixing of cold water in the mixed layer. Furthermore, the equatorial SST bias remotely contributes to the SST bias in the southeastern tropical Atlantic as well as a southward-shifted Angola-Benguela Front (Xu et al. 2014). The usage of unrealistic SSTs from ESMs in RCMs introduces biases in simulated precipitation over the African continent due to the sensitivity of RCMs to SST changes (e.g. Haensler et al. 2011; Weber et al. 2018a).

Two methods can be applied to reduce the SST bias in RCMs: (1) The SST can be adjusted by an empirical bias correction before its use as boundary condition in RCMs (e.g. Haensler et al. 2011; Hoffmann et al. 2016; Hernández-Díaz et al. 2017). This method works for reanalysis and historical simulations, but becomes difficult for climate change projections and leads to inconsistencies of the SST and the lower atmospheric fields over the ocean. (2) By regionally coupling the RCM with an ocean model that directly simulates the SST and allows for atmosphere–ocean interactions (e.g. Ratnam et al. 2015; Sein et al. 2015; Paxian et al. 2016; Cabos et al. 2017). However, this method requires high computational capacities because of the application of an atmosphere climate model and an ocean model that exchange certain variables in each time step via a coupler software.

Regional atmosphere–ocean coupling in RCMs has been applied and analyzed in various studies showing the benefits in different applications. The South Atlantic Anticyclone was identified as an important factor affecting the climate in southwestern Africa using the coupled model ROM (Cabos et al. 2017). Lengaigne et al. (2019) was able to reproduce the observed spatial–temporal distribution of tropical cyclones in the Indian Ocean with a regional coupled model. Furthermore, mesoscale wind systems over the coastal regions of southwestern Africa are well captured in coupled simulations, which also causes a reduction in the SST warm bias of the Benguela Current (Lima et al. 2019). Similarly, near-surface wind speed over the Canary Islands of the coast of Northwest Africa are better reproduced in coupled than in uncoupled simulations (Soares et al. 2019).

The application of regionally coupled atmosphere–ocean models also offers potential improvements in terms of simulated precipitation due to the given correlation between SST and precipitation over Africa (Washington and Preston 2006; van der Ent and Savenije 2013; Lutz et al. 2015). Spatial distributions of precipitation over southern Africa can be improved by coupling a simple mixed layer ocean model to the Advanced Research Weather Research and Forecast

Model (WRF) on the seasonal time scale (Ratnam et al. 2013). Paxian et al. (2016) reported that coupled regional models reduce the precipitation bias over the Guinea coast and central Sahel in decadal predictions. In addition, by comparing coupled and uncoupled models, Ratnam et al. (2015) showed that air–sea interactions are relevant processes in simulated precipitation during the peak season over southern Africa.

The above-mentioned studies with coupled RCMs already demonstrate the added value of atmosphere–ocean coupling in RCMs over the African continent, its coasts and offshore islands. However, there is still a lack of knowledge on the benefits of atmosphere–ocean coupling on precipitation over Africa in long-term regional climate projections. The objective of this work is to remedy this deficiency by analyzing the influence of atmosphere–ocean coupling on precipitation and its characteristics over Africa using the coupled model ROM, and answering the following questions: Which simulated precipitation characteristics, such as the annual cycle and selected precipitation indices, are improved by the coupling? Which coastal and continental regions of Africa will benefit? Finally, how does coupling affect climate change signals from precipitation indices in a regional climate projection? Answering these questions may help determine whether it is worth using a regional coupled atmosphere–ocean model to improve information on precipitation and its characteristics for certain African regions.

This study is structured as follows: Initially, the model experiments and the applied data sets are described in Sect. 2. The results of the analysis are presented and discussed in Sect. 3, and a conclusion will close this investigation in Sect. 4.

2 Models and data

2.1 Experiment setup

The simulations analyzed in this work were carried out using the regionally-coupled model ROM (Sein et al. 2015) and the atmospheric regional climate model REMO (Jacob 2001). As REMO is the atmospheric component of ROM, we can infer the benefits of atmosphere–ocean coupling by comparing their performance. The oceanic component of ROM is the Max Planck Institute Ocean Model (MPIOM; Marsland et al. 2003; Jungclaus et al. 2013). Both REMO (Déqué et al. 2012; Jacob et al. 2012; Kotlarski et al. 2014; Remedio et al. 2019; Teichmann et al. 2021) and ROM (Sein et al. 2014; Cabos et al. 2020; Soto-Navarro et al. 2020) have been used in different configurations to investigate the mechanism that govern the regional climate and the climate change signal around the world.

In MPIOM, the primitive equations are calculated on fixed z-levels in the vertical and on an orthogonal curvilinear Arakawa-C grid that can be stretched placing at least one of the model poles near/inside the area of coupling. These equations are solved using the Boussinesq and incompressibility approximations and a free-surface formulation. The possibility of stretching the grid allows us to achieve a spatial high resolution in the region of interest while maintaining a global domain at an acceptable computational cost, avoiding the problems associated with either open or closed boundaries typical of limited-area regional ocean models. In these simulations, we use the MPIOM grid TR04, which has a horizontal resolution that reaches up to 10 km (eddy permitting) near the coasts of Western Africa and decreases gradually, down to 30 km near the southern tip of the African continent and 100 km in the southern seas. In the vertical, MPIOM has 40 unevenly spaced z-levels, the thickness of which increases gradually from 16 m near the surface to 650 m for the deeper layer.

REMO has a dynamical core based on the Europa-Model of the German Meteorological Service (DWD; Majewski 1991) with physical parameterizations taken from versions 4 and 5 of the global climate model ECHAM (Roeckner et al. 1996, 2003). It uses a regular rotated grid with the equator positioned in the center of the model domain. Most of the prognostic variables of REMO are relaxed towards forcing data in the outer eight rows of the model area following Davies (1976). A radiative upper boundary condition is applied following Bougeault (1983) and Klemp and Durran (1983). In this work, we use a configuration of REMO that has a horizontal grid of 0.22° (25 km), with 31 vertical levels and a 120 s time step. The atmospheric domain chosen in this study covers most of the tropical Atlantic (see Fig. 1), as

well as parts of the Mediterranean and Indian Ocean, and is therefore larger than the CORDEX-Africa domain.

The global Hydrological Discharge model (HD, Hagemann and Dümenil Gates 2001) calculates river runoff globally and is coupled to both the atmosphere and ocean. REMO and MPIOM are coupled via the OASIS coupler (Valcke et al. 2003), which provides exchange between the ocean and atmosphere models with a 3-h coupling time step. More details about the coupling procedure can be found in Sein et al. (2015). Lateral atmospheric boundary conditions and upper oceanic forcing outside the coupled domain were prescribed using a historical simulation and a future projection with the low resolution configuration of the MPI-ESM earth system model (MPI-ESM-LR) under the CMIP5 Representative Concentration Pathway 8.5 (RCP8.5) scenario (Stevens et al. 2013). The RCP8.5 emission scenario assumes the worst case evolution of the emissions in the CMIP5 framework. This scenario leads in the long term to high energy demand and greenhouse gas emissions in absence of climate change policies (Riahi et al. 2011). In addition, REMO was driven with the ERA-INTERIM reanalysis data for evaluation purposes (Dee et al. 2011). This strategy allows us to analyse the influence of the coupling on the African precipitation in regional climate projections. A complete list of all experiments analyzed can be found in Table 1.

2.2 Observational and reanalysis data

Five different data sets are selected to assess the potential improvements in simulated SST, precipitation and derived precipitation indices. The diversity of the data product is intended to account for differences in the observational

Fig. 1 Model domain and orography [m] for REMO and ROM at a spatial resolution of 0.22° (red rectangle), and for MPIOM at a TR04 grid (black grid)

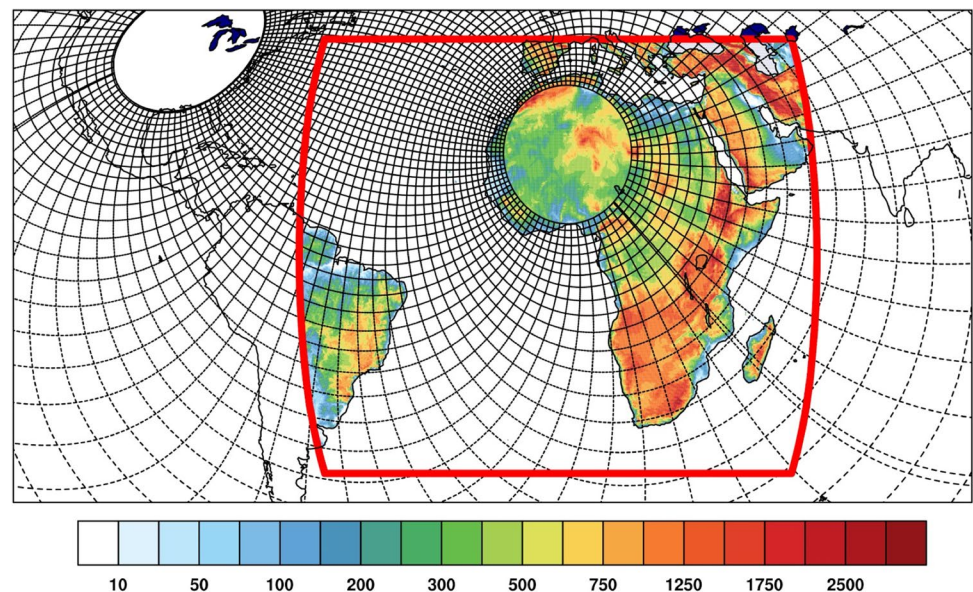


Table 1 Overview of the performed model simulations

Experiment	Model	Forcing data	Period	Ocean–atmosphere
REMO/ERA-INT	REMO	ERA-Interim reanalysis	1980–2014	Uncoupled
REMO/MPI-ESM-LR	REMO	MPI-ESM-LR, historical	1950–2005	Uncoupled
ROM/MPI-ESM-LR	ROM	MPI-ESM-LR, historical	1950–2005	Coupled
REMO/MPI-ESM-LR	REMO	MPI-ESM-LR, RCP8.5	2050–2099	Uncoupled
ROM/MPI-ESM-LR	ROM	MPI-ESM-LR, RCP8.5	2050–2099	Coupled

data sets for Africa (e.g. Sylla et al. 2013; Akinsanola et al. 2017). The NOAA OISST V2 data, which is available from September 1981 to present, with a spatial resolution of 0.25° (Reynolds et al. 2007; Huang et al. 2021) and the SST from the ERA5 reanalysis data set from the Copernicus Climate Change Service (C3S) Climate Data Store (CDS) for the period 1979 to present with a spatial resolution of 0.25° (Hersbach et al. 2018, 2020) are used to assess the simulated SSTs by ESM and ROM. The University of East Anglia Climatic Research Unit (CRU) data set version TS 4.05 (Harris et al. 2020), covering the period 1901–2020 with a spatial resolution of 0.5° , and the Global Precipitation Climatology Centre (GPCC) V2020 starting from the period 1891–2019 with a spatial resolution of 0.25° (Schneider et al. 2020), are applied to evaluate the simulated precipitation. Moreover, the precipitation data from the Climate Hazards group Infrared Precipitation with Stations (CHIRPS) V2.0 starting from 1981 to present with a spatial resolution of 0.25° (Funk et al. 2014, 2015) and from the ERA5 reanalysis data set (Hersbach et al. 2018, 2020) are also used.

3 Results and discussion

For a comprehensive overview of the influence of the regional atmosphere–ocean coupling on precipitation and its characteristics over Africa, we analyze the seasonal mean sea surface temperature (SST) bias, seasonal mean vertical integrated moisture transport and seasonal mean daily precipitation using the MPI-ESM-LR driven simulations. Furthermore, we assess the improvements in simulating precipitation by measuring the added value of seasonal mean daily precipitation related to the data sets

CRU, GPCC, CHIRPS and ERA5, and the annual precipitation cycle compared to the data sets CRU, GPCC and CHIRPS for different African sub-regions. Moreover, normalized daily precipitation distributions of REMO forced by ERA-INT and MPI-ESM-LR, and ROM forced by MPI-ESM-LR are also analyzed and compared to CHIRPS and ERA5. In addition, precipitation indices (see Table 2) derived from model simulations are evaluated using CHIRPS from 1981 to 2005, and modifications of these indices are examined under a high emissions scenario by the end of the century (2070–2099).

Daily precipitation is analysed using normalized precipitation distributions, as applied by Soares and Cardoso (2018), which only consider precipitation on wet days (days with ≥ 1 mm). They argued that using normalised precipitation is a more consistent way to show precipitation differences, as each bin containing normalised precipitation amounts represents a fraction of the total precipitation. To calculate the distributions, bins with a width of 1 mm/day are defined and the frequency of each bin is multiplied by the mean bin width to obtain the amount of precipitation. Subsequently, the precipitation amount of each bin is normalized by dividing each bin by the total precipitation sum calculated over all bins.

In order to measure the added value of the regional atmosphere–ocean coupling on simulated precipitation using CRU, GPCC, CHIRPS and ERA5, we apply the adapted formula of Dosio et al. (2015) as follows:

$$AV = \frac{(REMO - REF)^2 - (ROM - REF)^2}{MAX[(REMO - REF)^2, (ROM - REF)^2]}, \quad (1)$$

Table 2 Overview of analyzed precipitation indices

Index	ID	Definition	Unit
Maximum number of consecutive dry days	CDD	Maximum number of consecutive days with < 1 mm precipitation	days
Maximum number of consecutive wet days	CWD	Maximum number of consecutive days with ≥ 1 mm precipitation	days
Number of annual dry days	DD	Annual sum of days with < 1 mm precipitation	days
Annual total wet day precipitation	PRCPTOT	Annual total precipitation on days ≥ 1 mm precipitation	mm
Annual total precipitation on wet days > 95 th percentile	R95p	Annual total precipitation when > 95 th percentile on days ≥ 1 mm	mm
Annual total precipitation on wet days > 99 th percentile	R99p	Annual total precipitation when > 99 th percentile on days ≥ 1 mm	mm

where AV is the added value, REMO and ROM are the simulated precipitation of the models, and REF is the respective precipitation reference data set at each grid box.

3.1 Seasonal warm and cold sea surface temperature bias

A comparison of the sea surface temperatures (SSTs) in the MPI-ESM and ROM historical simulations with the

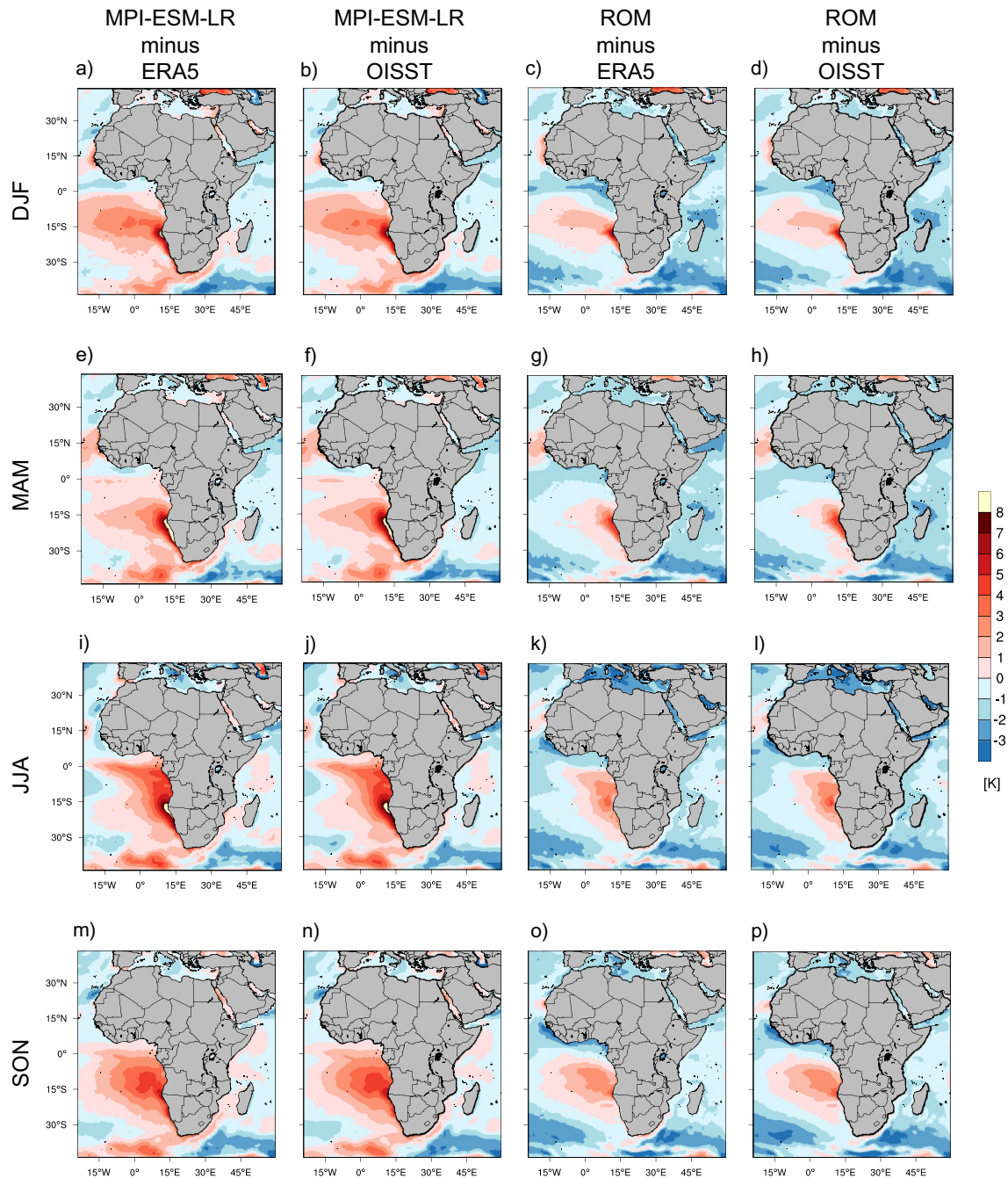


Fig. 2 Seasonal mean sea surface temperature (SST) bias [K] simulated by MPI-ESM-LR (first two columns), which is used as forcing for REMO, and by ROM (third and fourth column) compared to

ERA5 from 1981 to 2005 and OISST V2 from 1982 to 2005 for **a–d** December to February (DJF), **e–h** March to May (MAM), **i–l** July to August (JJA) and **m–p** September to November (SON)

SSTs from ERA5 and OISST shows that, regardless of the reference datasets used, the SST patterns of warm and cold biases are almost similar in terms of strength and location (Fig. 2a–p). The highest warm bias occurs along the upwelling areas of the Benguela current offshore the Namibian and Angolan coasts with more than +8 K in DJF, MAM and JJA (Fig. 2a, b, e, f, i, j) and a bias with up to +6 K in SON (Fig. 2m, n). In all seasons, there is a west–east gradient in the SST bias recognizable. A warm SST bias is also observed, but to a lesser extent, offshore along the Agulhas current up the Mozambique Channel in the Indian Ocean with up to +3 K in DJF and MAM (Fig. 2a, b, e, f). A cold SST bias is found in the Indian Ocean south of 30°S with more than +3 K (Fig. 2a, b, e, f, i, j, m, n). The warm SST bias in the Southeast Atlantic in the MPI-ESM model has already been reported by other studies (Haensler et al. 2011; Paxian et al. 2016; Eichhorn and Bader 2017; Weber et al. 2018a) and which is a common problem in coupled CMIP5 models (e.g. Toniazzo and Woolnough 2014; Xu et al. 2014; Găinușă-Bogdan et al. 2018).

By applying the regional coupled atmosphere–ocean model ROM, the warm SST biases in the Southeast Atlantic Ocean and in the Southwest Indian Ocean are reduced both in its absolute values and in its spatial extent in all seasons (Fig. 2c, d, g, h, k, l, o, p). The highest warm SST bias is observed with up to +7 K in DJF (Fig. 2c, d) and a reduced bias with up to +5 K in JJA and SON (Fig. 2k, l, o, p) offshore the Namibian and Angolan coasts in the Southeast Atlantic. The Agulhas current in the Southwest Indian Ocean exhibits the highest warm SST bias with up to +2 K (Fig. 2c, d, g, h, k, l, o, p). In all seasons, the cold SST bias in the South Atlantic and Indian Ocean becomes somewhat larger with more than -3 K. Cold biases can also be seen along the West African coast, Northern Madagascar and the Mediterranean Sea in single seasons.

The reduction in the warm bias in the Southeast Atlantic Ocean is most likely a result of the improved representation of the Benguela upwelling region and the inclusion of atmosphere–ocean interactions in the coupled model ROM. De la Vara et al. (2020) showed that refinements of both atmospheric and oceanic model grids achieves the best results in simulating the SST of the Benguela and Agulhas currents. They also explained that the remaining warm bias is more likely caused by an incorrect vertical temperature profile in the ocean than an insufficiently modelled upwelling in these regions. In addition, the cold SST bias in the Canary upwelling system in ROM was also reduced compared to the MPI-ESM simulation. The improvement in simulated SST in both the Benguela and Canary upwelling systems can be considered as a direct effect of the higher oceanic resolution in the ROM (Fig. 1).

3.2 Moisture transport and seasonal precipitation

Reduced warm SST biases simulated by ROM in the Southeast Atlantic and Southwest Indian Oceans affect the large-scale circulation, and the vertically integrated moisture transport (VIMT) across West Africa in JJA and in southern Africa in DJF (Fig. 3a–f). In the historical simulation of the coupled model ROM, the VIMT moving from the Atlantic Ocean onshore the West African coast is attenuated and more directed towards Northeast compared to uncoupled model REMO (Fig. 3b, d, f). The VIMT from east to west over the Sahel is also lower, indicating a weakening of the African Easterly Jet (AEJ).

This leads to changes in precipitation in terms of absolute and relative values over West Africa (Figs. 4a–d, 5a–d). In the ROM simulation, precipitation decreases between -15 to -5 mm/day over the Gulf of Guinea and less than -15 mm/day offshore the coasts of Cameroon and Equatorial Guinea in JJA (Fig. 4c). Furthermore, precipitation decreases in JJA and SON between -15 to -0.5 mm/day over the countries along the Gulf of Guinea from Guinea to Gabon and further to Angola with a strong gradient of precipitation reduction towards the coast (Fig. 4c, d). The relative change in precipitation is up to -100% less precipitation over coastal regions of North Africa, in all seasons (Fig. 5a–d), and over coastal regions of West Africa from Guinea to Cameroon in JJA and SON (Fig. 5c, d). In contrast, an increase in precipitation is simulated between +0.5 and +5 mm/day along 15°N over the African continent with the highest amount over West Africa (Fig. 4c).

The described meridional precipitation pattern over West Africa in JJA, which shows a decrease in the South and an increase in the North, suggests that the Inter Tropical Convergence Zone (ITCZ) moves further northward in the simulation with the regional coupled atmosphere–ocean model ROM than in uncoupled model REMO. The northward shift of the ITCZ could be caused by a colder SST (Fig. 2k, l), which coincides with higher sea-level pressure and less evaporation of moisture in the Gulf of Guinea (not shown), and by the change in VIMT over West Africa.

Over the Southeast Atlantic in DJF, the VIMT has weakened onshore along the Angolan coast due to an intensified high-pressure system over the South Atlantic and to a colder SST in ROM (Fig. 3a, c, e). Weber et al. (2018a) found similar results in sensitivity experiments with REMO using bias-corrected SSTs, and showed that colder SSTs reduce ascending air offshore the Angolan coast. Cabos et al. (2017) have already demonstrated that the strength of the South Atlantic Anticyclone and SST changes due to atmosphere–ocean interactions are correlated in this region. Over the West Indian Ocean in DJF, the VIMT, which moves along offshore the African coast from the Horn of Africa to Tanzania and points to Northern Madagascar, is weaker in ROM compared

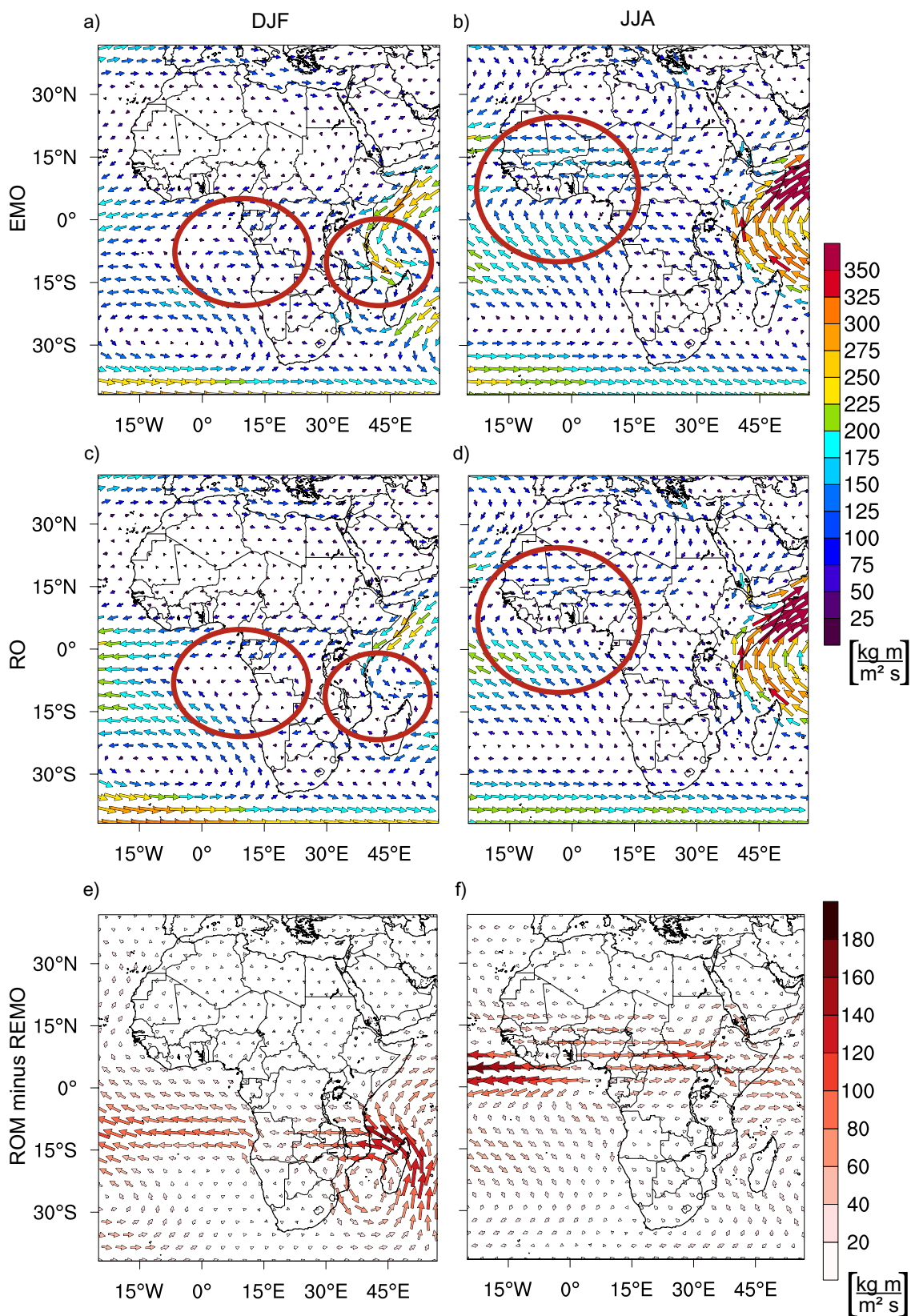


Fig. 3 Seasonal mean vertical integrated moisture transport [$\text{kg m} / \text{m}^2 \text{ s}$] for December to February (DJF) (first column) and July to August (JJA) (second column) from 1971 to 2000. **a, b** REMO forced

with MPI-ESM-LR and **c, d** ROM forced with MPI-ESM-LR and **e, f** vector differences ROM minus REMO. The red circles are the regions of interest that show larger vector differences

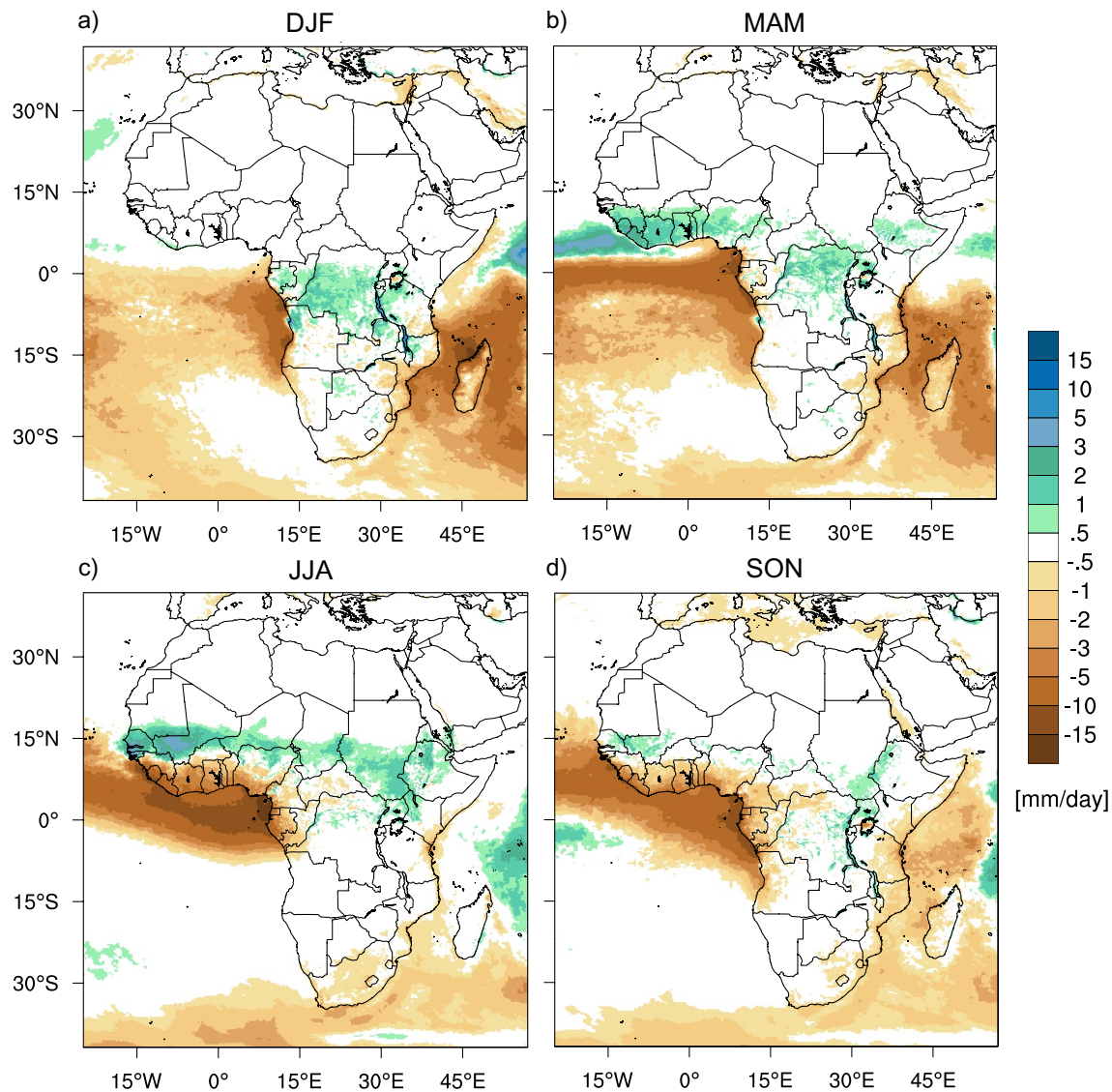


Fig. 4 Absolute differences in seasonal mean precipitation [mm/day] of ROM minus REMO, both forced with MPI-ESM-LR for **a** December to February (DJF), **b** March to May (MAM), **c** July to August (JJA) and **d** September to November (SON) from 1971 to 2000

to REMO (Fig. 3a, c, e). Weber et al. (2018a) obtained an opposite result, showing an increase in VIMT in this region by correcting only the SST in REMO. The weaker VIMT over the West Indian Ocean in ROM appears to be a result of atmosphere–ocean interactions, which are possible in ROM and not in REMO.

The reduced VIMT onshore along the Angolan coast and along the east African coast leads to a lower moisture supply and to less precipitation over the continent south of the equator. In the ROM simulation, there is up to -100% less precipitation over coastal regions of southern Africa, especially Southwest Africa, and Madagascar in all seasons, with the exceptions of Eastern Madagascar in JJA and SON showing an increase up to 50% (Fig. 5c, d). The strong relative

changes in precipitation over the whole of southern Africa in the JJA are a result of the low absolute precipitation values in these regions (Fig. 5a–d). On the contrary, ROM simulates up to 100% more precipitation over Central Africa and up to 50% more precipitation in the inner parts of southern Africa in DJF and MAM (Fig. 5a, b).

Of particular interest are the islands offshore the African continent, since the SST of the surrounding oceans strongly affects the precipitation over the islands. Due to the grid spacing of about 25 km in the atmospheric model, small islands are only represented by a few grid boxes. However, it is worth considering them in this analysis in order to estimate the possible changes in precipitation over the islands. There are distinct differences between ROM and

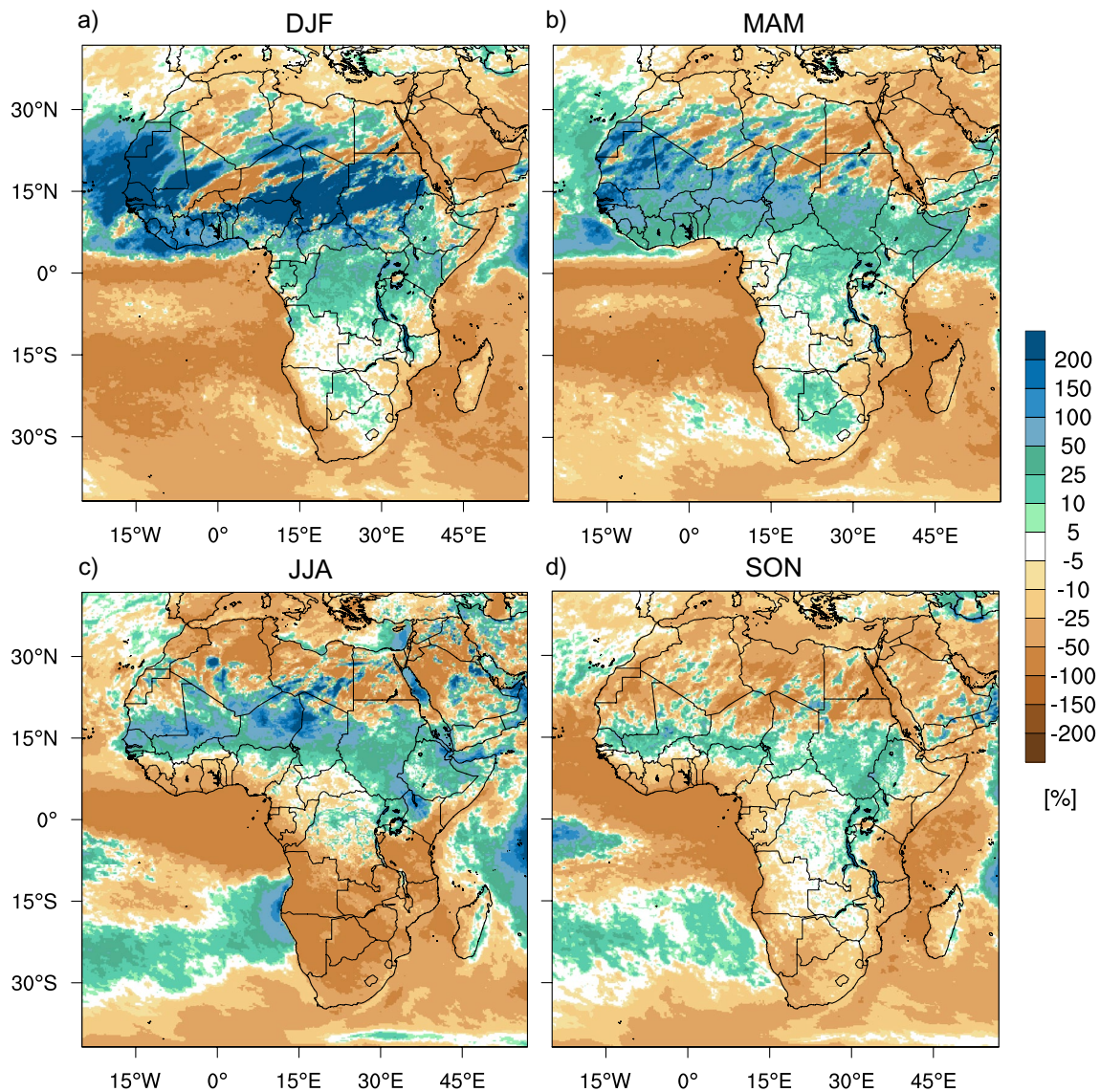


Fig. 5 Relative differences in seasonal mean daily precipitation [%] of ROM minus REMO, both forced with MPI-ESM-LR for **a** December to February (DJF), **b** March to May (MAM), **c** July to August (JJA) and **d** September to November (SON) from 1971 to 2000

REMO in the simulation of precipitation over the islands located close to the African continent. Over the Atlantic Ocean, ROM simulates precipitation changes compared to REMO between -100 and $+100\%$ over the Canary Islands and between -100 and -25% over São Tomé and Príncipe during the year (Fig. 5a–d). Over the Indian Ocean, precipitation in ROM decreases up to -100% over the Comoros and over Mayotte in the different seasons (Fig. 5a–d). The decrease (increase) in precipitation over the islands coincides with lower (higher) SST values, resulting in lower (higher) evaporation of moisture over the surrounding sea surfaces (not shown). Therefore, it is urgent that model simulations of precipitation over islands either use bias-corrected SSTs of the surrounding oceans or use a regionally coupled

atmosphere–ocean model that provides SSTs directly from the ocean model with higher resolution.

3.3 Added value of seasonal mean daily precipitation

To assess the potential improvements in reducing the precipitation bias over Africa and the islands near the African continent by applying a regionally coupled atmosphere–ocean model, the added value AV was determined for each grid box using (Eq. 1). Simulated precipitation by REMO and ROM is compared to the observational data sets CRU, GPCC, CHIRPS and the ERA5 reanalysis data set to account for the lack of observational stations over Africa and the resulting

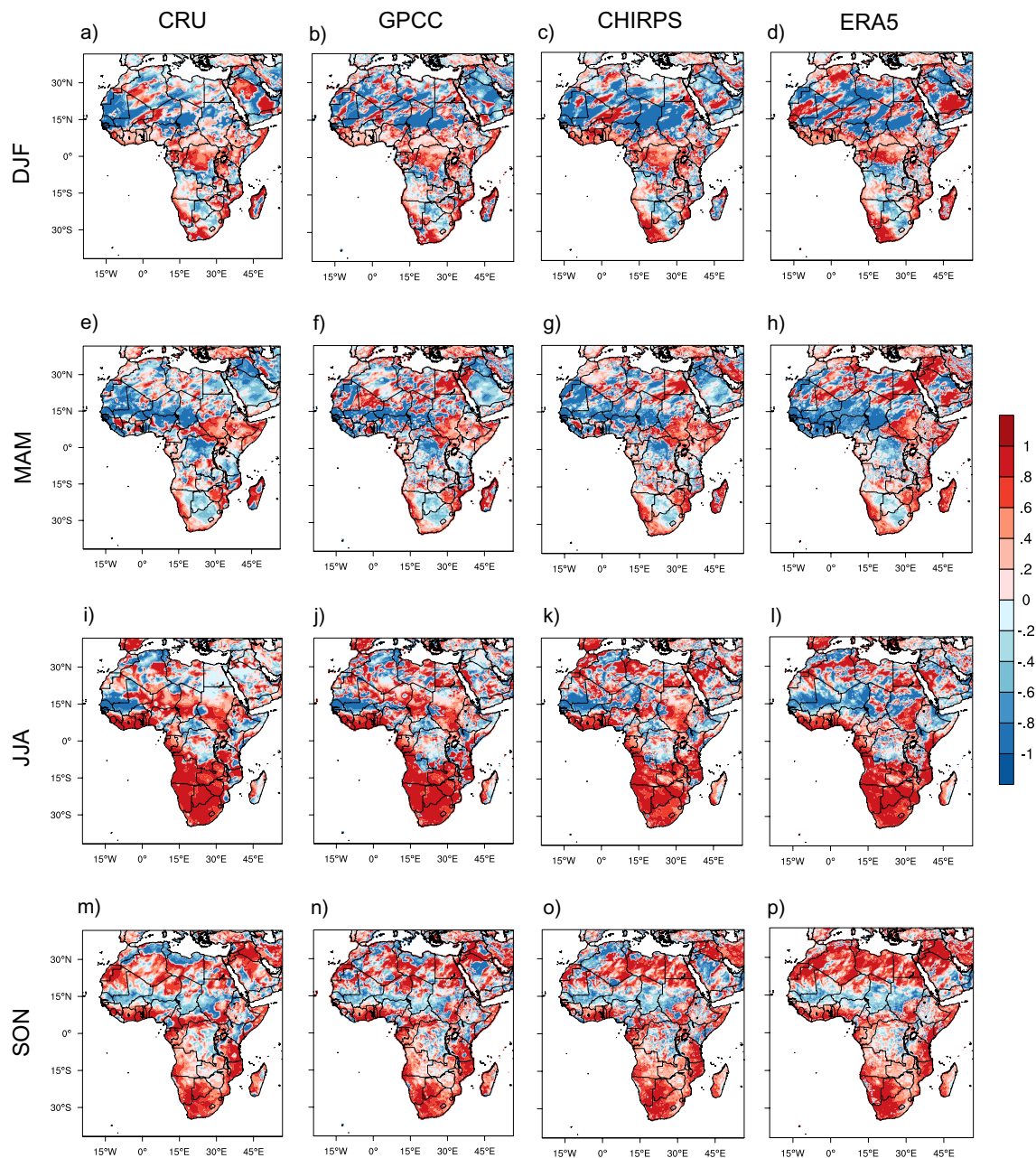


Fig. 6 Added value AV of seasonal mean daily precipitation for entire Africa in ROM compared to REMO forced with MPI-ESM-LR. Reference data sets are CRU TS 4.05 and GPCC V2020 from 1971 to 2000, CHIRPS V2.0 and ERA5 from 1981 to 2005 for **a–d** Decem-

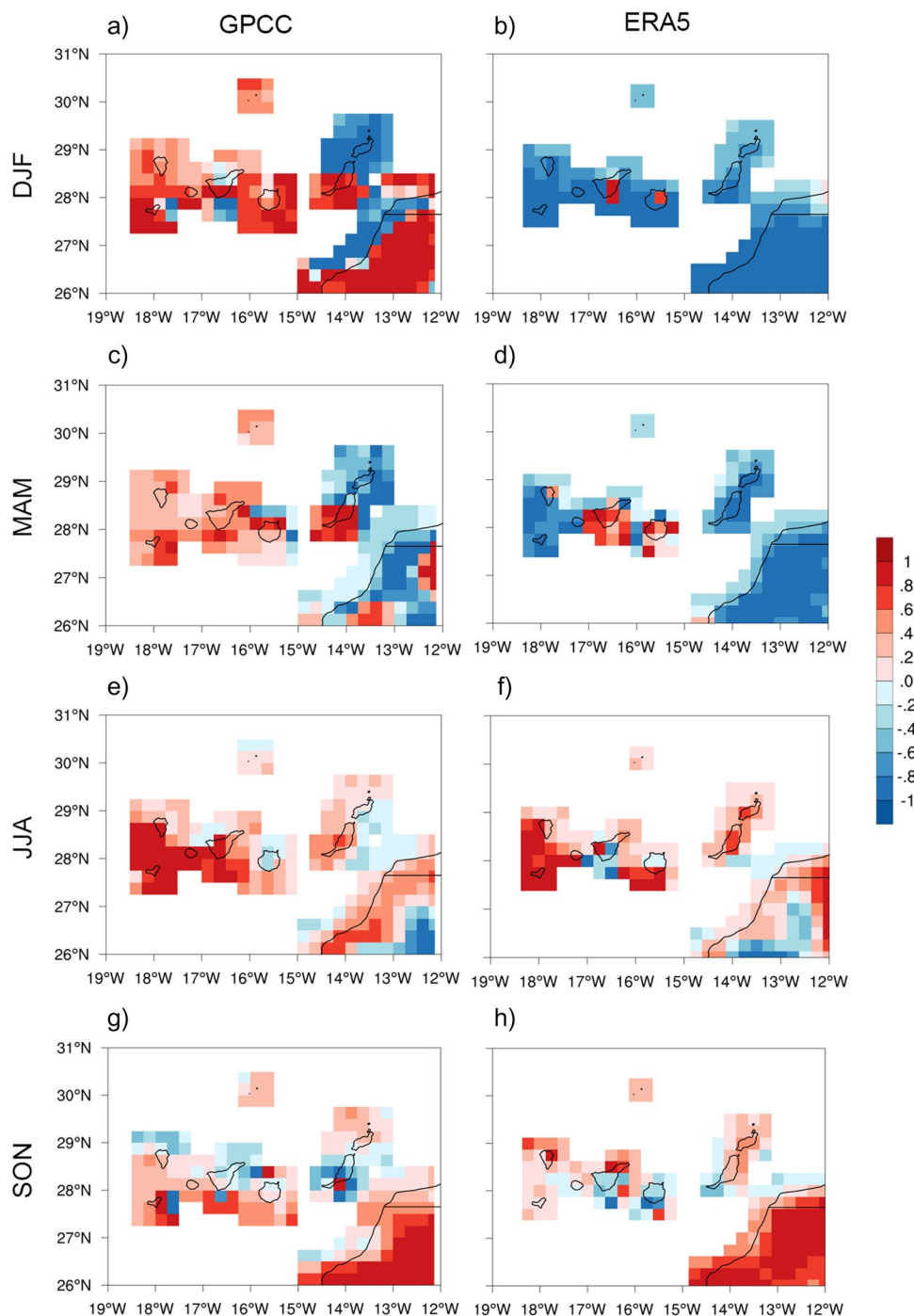
ber to February (DJF), **e–h** March to May (MAM), **i–l** July to August (JJA) and **m–p** September to November (SON). Positive (negative) values indicate a lower (higher) precipitation bias of ROM compared to REMO

inadequacies in the observational data sets (Figs. 6a–p, 7a–h, 8a–h, 9a–h). Positive (negative) values indicate a lower (higher) precipitation bias of ROM compared to REMO. In detail, an AV of +1 indicates that the precipitation bias of ROM is zero, while an AV of -1 indicates that the precipitation bias of REMO is zero.

It can be seen that the patterns of precipitation bias in the different reference datasets are almost identical and are

therefore independent of the reference data used for the African continent (Fig. 6a–p). The bias in ROM is reduced mainly over North Sahara in SON, over most coastal regions of Sub-Saharan Africa in all seasons, over Central Africa in DJF, over southern Africa in JJA and SON, and over the entire Greater Horn of Africa in MAM. In particular, the inner parts of southern Africa show less precipitation in JJA with a distinct bias reduction (Figs. 5c, 6i–l). However, it

Fig. 7 Added value AV of seasonal mean daily precipitation for the Canary Islands in ROM compared to REMO forced with MPI-ESM-LR. Reference data sets are GPCP V2020 from 1971 to 2000 and ERA5 from 1981 to 2005 for **a, b** December to February (DJF), **c, d** March to May (MAM), **e, f** July to August (JJA) and **g, h** September to November (SON). Positive (negative) values indicate a lower (higher) precipitation bias of ROM compared to REMO



has to be kept in mind that there is generally little precipitation during this time of year due to the dry season. Furthermore, ROM decreases the precipitation bias over most parts of Madagascar from SON to MAM. In contrast, the precipitation bias increases in ROM over most regions north of 10° N and over the interior of southern Africa in DJF and MAM, over Central Africa in MAM, and along 15° N in SON. The reduction in precipitation bias in the coastal regions of West Africa is confirmed by Paxian et al. (2016),

who found a reduced precipitation bias in decadal climate predictions for the Guinea Coast with a regionally coupled atmosphere–ocean model. Furthermore, it has been shown by Haensler et al. (2011) and Weber et al. (2018a) that the application of a bias-corrected SST leads to improved precipitation results in regional climate models over southern Africa.

Assessing the utility of a regionally coupled atmosphere–ocean model over small islands is difficult due to

Fig. 8 Added value AV of seasonal mean daily precipitation for Comoros and Mayotte in ROM compared to REMO forced with MPI-ESM-LR. Reference data sets are GPCC V2020 from 1971 to 2000 and ERA5 from 1981 to 2005 for **a**, **b** December to February (DJF), **c**, **d** March to May (MAM), **e**, **f** July to August (JJA) and **g**, **h** September to November (SON). Positive (negative) values indicate a lower (higher) precipitation bias of ROM compared to REMO

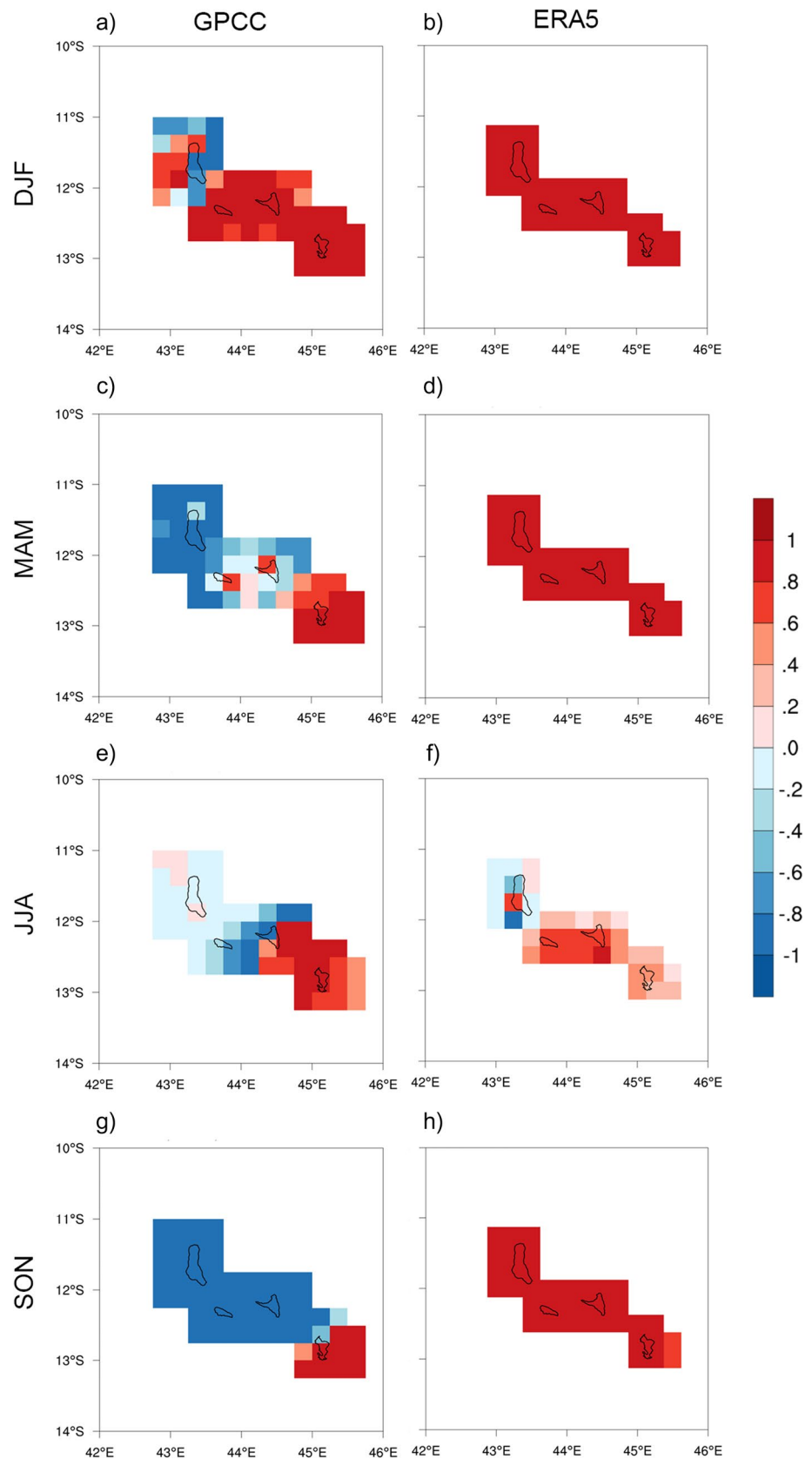
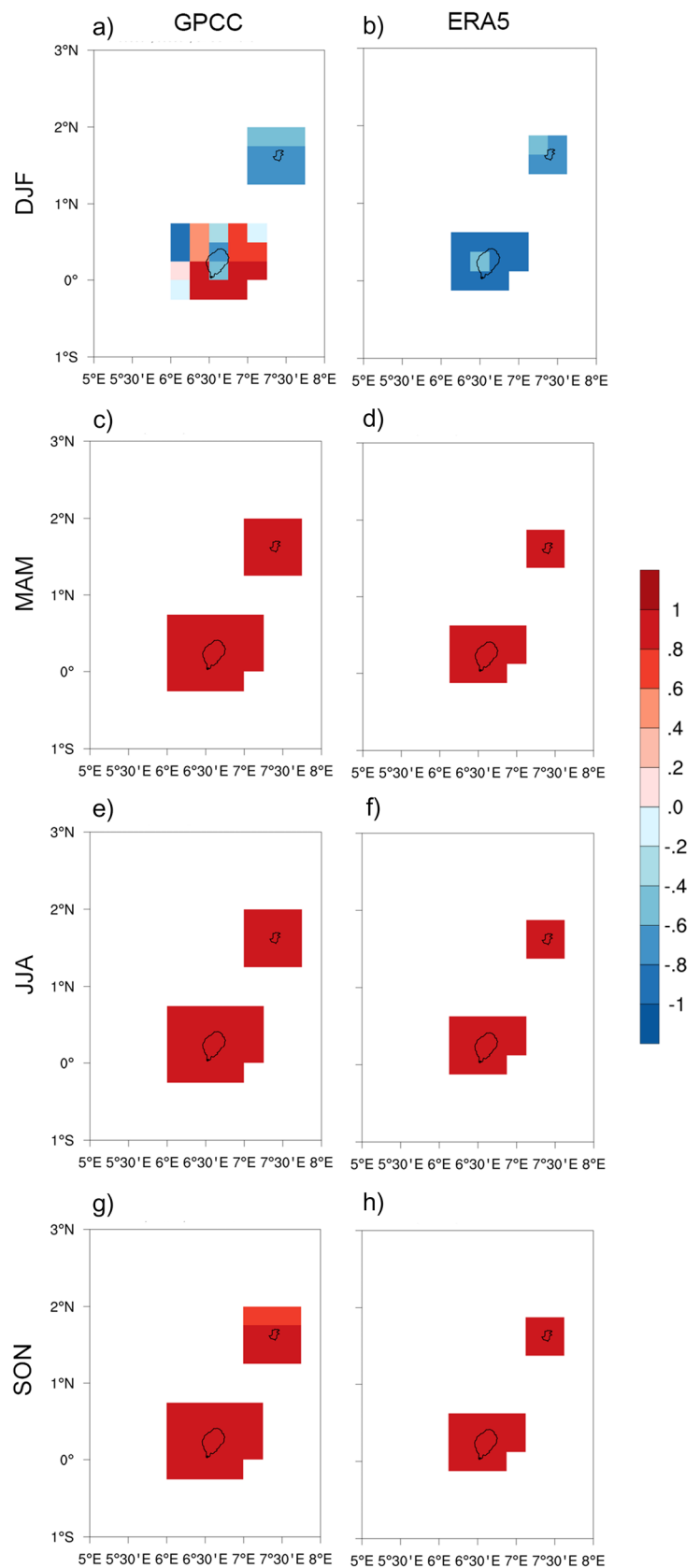


Fig. 9 Added value AV of seasonal mean daily precipitation for São Tomé and Príncipe in ROM compared to REMO forced with MPI-ESM-LR. Reference data sets are GPCC V2020 from 1971 to 2000 and ERA5 from 1981 to 2005 for **a**, **b** December to February (DJF), **c**, **d** March to May (MAM), **e**, **f** July to August (JJA) and **g**, **h** September to November (SON). Positive (negative) values indicate a lower (higher) precipitation bias of ROM compared to REMO



the scarcity of reference data. Only the GPCP precipitation dataset and the ERA5 reanalysis data set provide some gridded information on precipitation over the Canary Islands, São Tomé and Príncipe, Comoros and Mayotte with a spatial resolution of 0.25° (about 28 km). Over the Canary Islands, GPCP shows some minor precipitation biases in ROM, mainly for the western islands in all seasons, while ERA5 shows mainly a reduction in biases for JJA and SON (Fig. 7a–h). In contrast, ERA5 indicates a reduction in precipitation biases in ROM over Comoros and Mayotte for all seasons, while GPCP indicates only an improvement of simulated precipitation over Mayotte in all seasons and only some improvements over Comoros from DJF to JJA (Fig. 8a–h). Over São Tomé and Príncipe, both ERA5 and GPCP show reduced precipitation biases in ROM only from MAM to SON (Fig. 9c–h). Despite some inconsistencies in the reference data GPCP and ERA5, the results show that the regionally coupled atmosphere–ocean model ROM can reduce the precipitation bias over these island groups compared to the atmosphere-only model REMO.

3.4 Regional precipitation characteristics

A main aspect of this work is to investigate to what extent the precipitation characteristics in certain regions of the African continent are influenced by the regional atmosphere–ocean coupling. For this purpose, eight different sub-regions were defined, located along the coast and in

the interior of the continent (Fig. 10). The sub-regions are labeled as follows: West Africa North (WAN), West Africa South (WAS), Equatorial Africa (EQA), East African Coast (EAC), Southwest Africa North (SWN), Southwest Africa South (SWS), Botswana (BOT), and Western Cape Region (WCR). For each of these sub-regions, the annual precipitation cycle, the normalized daily precipitation distribution and the following precipitation indices were calculated and analyzed as region averages: the maximum number of consecutive dry days (CCD), the maximum number of consecutive wet days (CWD), the number of annual dry days (DD), total annual precipitation on wet days (PRCPTOT), annual precipitation > 95th percentile (R95p), and annual precipitation > 99th percentile (R99p) (Table 1).

3.4.1 Evaluation of the annual precipitation cycle

Simulated annual precipitation cycles in the historical simulations of ROM and REMO, and in the ERA-INT driven simulation of REMO are compared with the cycles derived from CRU, CHIRPS and GPCP. The analysis shows that the annual precipitation cycles simulated with ROM are mainly closer to observations in coastal regions than in the interior of the continent (Fig. 11a–h). Over regions along the Guinea Coast of West Africa (WAS), ROM is able to reproduce a bimodal annual precipitation cycle in the historical simulation, which cannot be achieved with REMO (Fig. 11b). Furthermore, the simulated bimodal precipitation cycle in ROM is closer to observations from June to November. Interestingly, the ERA-INT-driven simulation of REMO also shows a bimodal precipitation cycle, but with higher peaks compared to ROM and which deviate significantly from the observed data. This suggests that the enabled process of atmosphere–ocean interaction in ROM has a dampening effect on the two precipitation peaks.

The coastal regions of Southwest Africa North (SWN) except March, Southwest Africa South (SWS) and Western Cape Region (WCR) experience less precipitation in the historical simulation of ROM being closer to observations than in REMO (Fig. 11e, f, h). In these regions, the precipitation cycles in the ERA-INT-driven REMO simulation show the best agreement with the observations. The difference between the precipitation cycles in the ROM and in the ERA-INT driven REMO simulation is due to the persistent warm SST bias in the ROM, which favours evaporation over the ocean and moisture transport along the Angolan coast (e.g. Weber et al. 2018a). Over the East African Coast (EAC), ROM simulates significantly less precipitation in the historical run compared to REMO, but with better agreement with observations from May to December and slightly worse agreement from January to March (Fig. 11d). From October

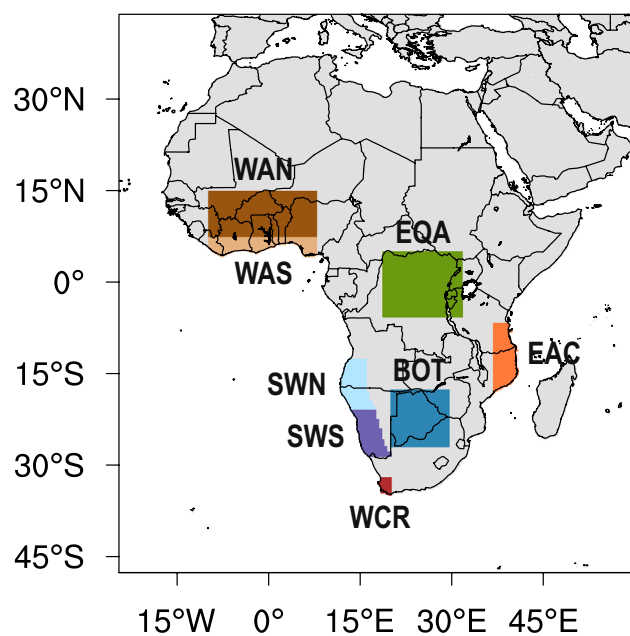
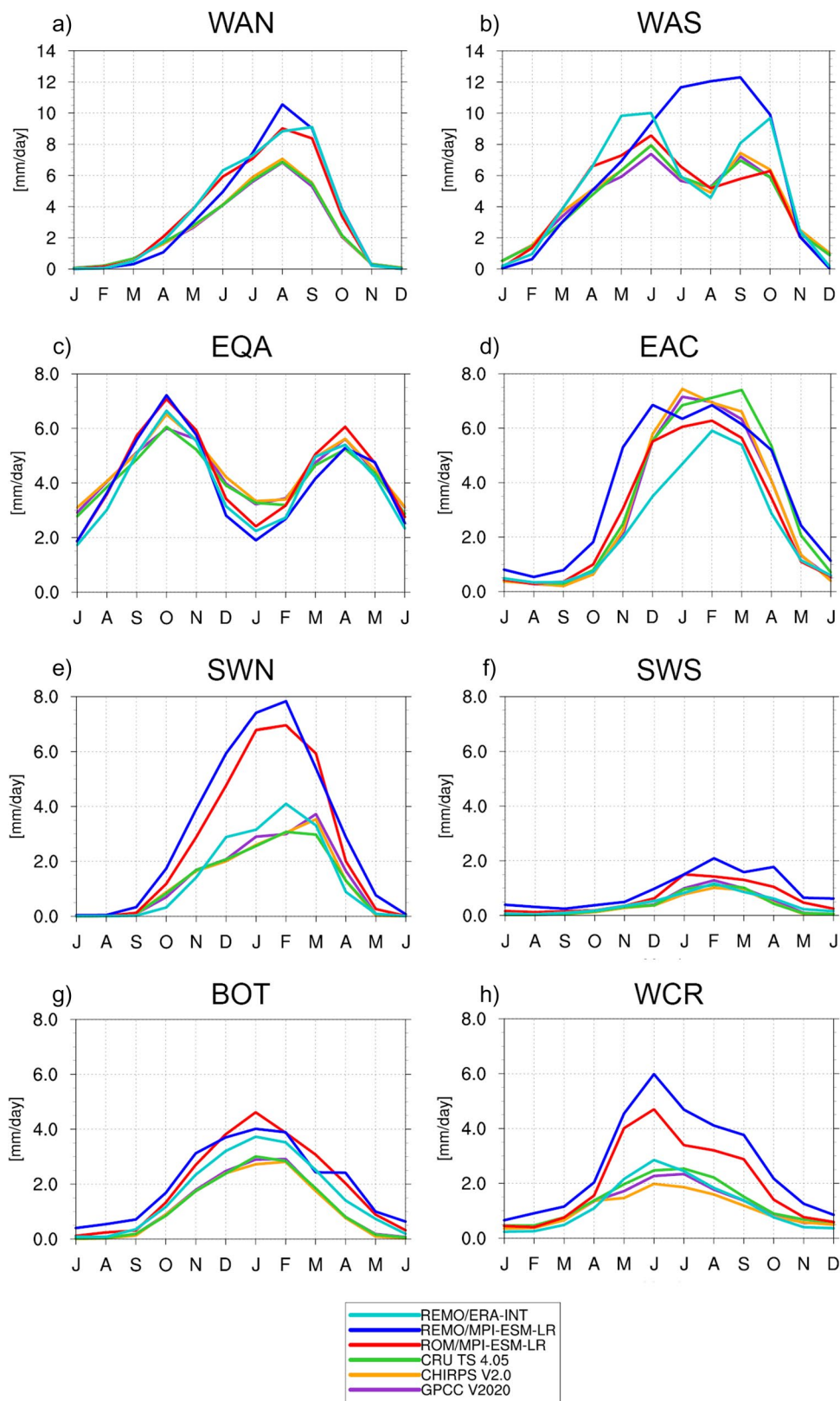


Fig. 10 African sub-regions: West Africa North (WAN), West Africa South (WAS), Equatorial Africa (EQA), East African Coast (EAC), Southwest Africa North (SWN), Southwest Africa South (SWS), Botswana (BOT), Western Cape Region (WCR)

Fig. 11 Annual precipitation cycles simulated by REMO forced with ERA-INT (cyan), and by REMO (blue) and ROM (red) both forced with MPI-ESM-LR for different African sub-regions from 1981 to 2005 compared to CRU TS 4.05 (green), CHIRPS V2.0 (orange) and GPCC V2020 (purple)



to April, the ERA-INT driven REMO simulation shows less precipitation than ROM, although ROM has a small cold SST bias. This could indicate that the SST has a smaller

impact on precipitation in this region and that the difference in precipitation between ROM and the ERA-INT driven

REMO simulation is the result of the changes in moisture transport.

Over the interior regions of the continent, Equatorial Africa (EQA) and Botswana (BOT), annual precipitation cycles in the historical simulations of ROM and REMO are essentially similar, except that ROM shows more precipitation in EQA from December to April and slightly less precipitation from April to November in BOT (Fig. 11c, g). The same applies to the northern parts of West Africa (WAN), where ROM shows slightly more precipitation from March to June compared to REMO in the historical simulation, but less from July to October (Fig. 11a). These results suggest a smaller influence of the reduced warm SST biases in the surrounding oceans on precipitation over the northern parts of West Africa (WAN), Equatorial Africa (EQA) and Botswana (BOT).

3.4.2 Evaluation of daily precipitation

To analyse the influence of atmosphere–ocean coupling on daily precipitation, the normalized daily precipitation distributions calculated from historical simulations of ROM and REMO, and from the ERA-INT-driven simulation of REMO are compared with the distributions derived from CHIRPS and ERA5 (Fig. 12a–h). In most sub-regions, the precipitation frequency maxima of ROM and REMO are lower than those of CHIRPS and ERA5 in the historical simulations, which are in the range of small precipitation amounts. However, ROM simulates small daily precipitation amounts more frequently and larger amounts less frequently compared to REMO in the coastal regions of West Africa (WAS), Southwest Africa (SWN and SWS), and Western Cape Region (WCR), and in the inner parts of West Africa (WAN) and Botswana (BOT) (Fig. 12a, b, e–h). In particular, the differences in the precipitation distributions of the historical simulations between ROM and REMO are most pronounced in the coastal regions of WAS, SWN and SWS, indicating a direct impact of the lower warm SST bias in the Southeast Atlantic on daily precipitation (Fig. 12b, e, f). Distinct effects of the fully removed warm SST bias can be seen in the ERA-INT driven simulation of REMO in SWN and SWS, where the precipitation distributions are closest to those of CHIRPS and ERA5 (Fig. 12e, f).

SST biases in the oceans appear to have less influence on daily precipitation in the regional climate model simulations over equatorial Africa (EQA), as the distributions in this region are close to each other (Fig. 12c). A striking feature of the results is the significant difference in daily precipitation between ERA5 and CHIRPS, especially in WAS and EAC (Fig. 12b, d). In these regions, the precipitation frequency maxima of ERA5 are significantly higher than the ones of CHIRPS, with CHIRPS having more frequent higher daily precipitation amounts than ERA5. The differences in

daily precipitation between the ERA5 reanalysis data set and CHIRPS should be further investigated, but this is beyond the scope of this work.

3.4.3 Evaluation of precipitation indices

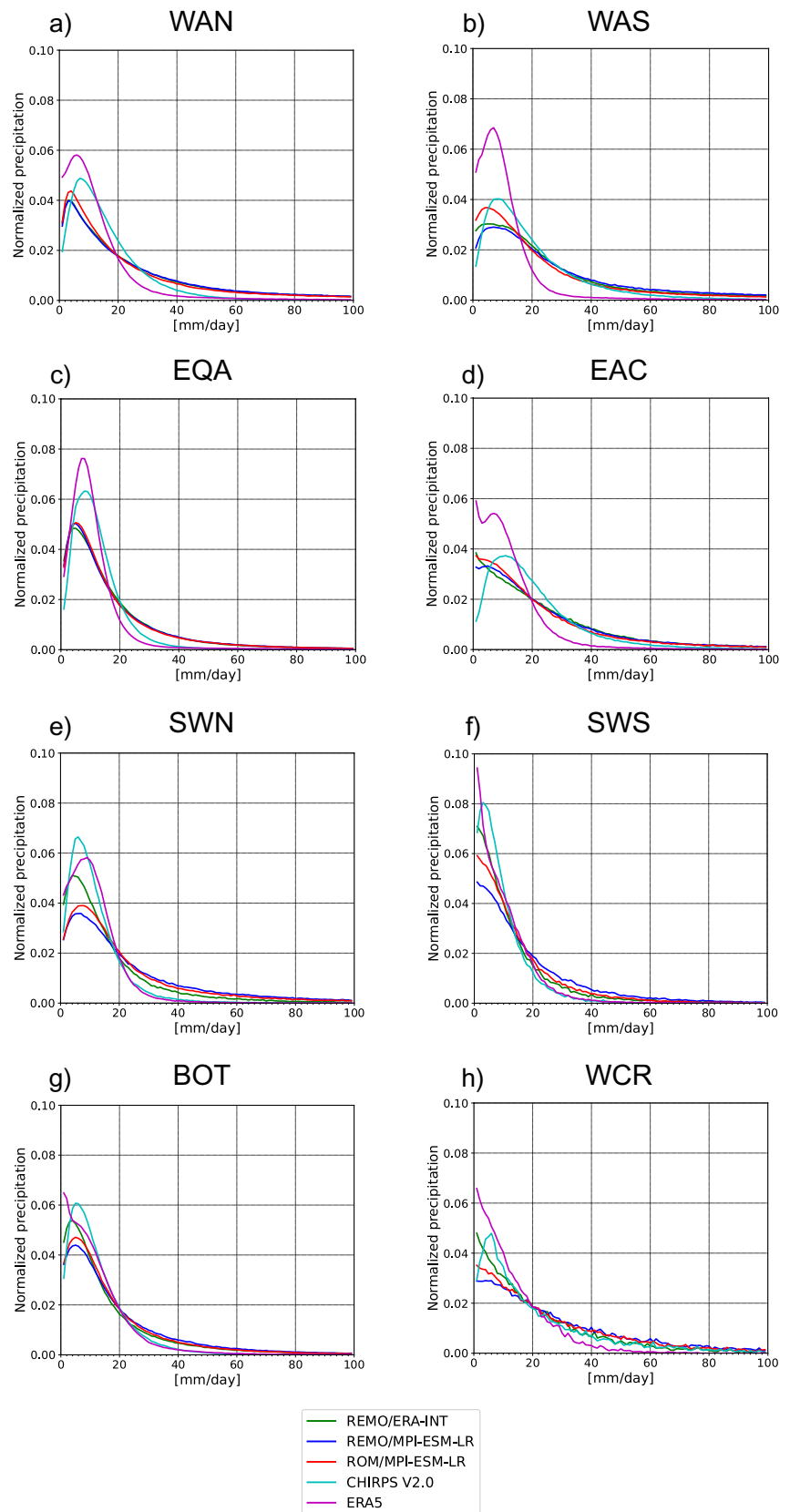
By analyzing selected precipitation indices derived from historical simulations of ROM and REMO, from the ERA-INT driven REMO simulation, and from the observational data set CHIRPS, more detailed information on the influence of regional atmosphere–ocean coupling on precipitation characteristics can be obtained. The number of annual dry days (DD) shows a change of -4 and $+4\%$ over West Africa (WAN, WAS), and a decrease of -7% over equatorial Africa (EQA) in the historical simulation of ROM compared to REMO (Fig. 13a). For the East African Coast (EAC) and southern Africa (SWN, SWS, WCR), the coupled model simulates an increase in DD between $+3$ and $+9\%$ compared to the uncoupled model, with the coupled model results being closer to both observations and the ERA-INT driven simulation of REMO.

Similar regional differences between the coupled and uncoupled model arise in the simulation of the maximum number of consecutive dry days (CDD). ROM simulates a decrease in CDD of -7 and -13% over West Africa (WAN, WAS), an increase between $+10$ and $+38\%$ over the East African Coast (EAC) and southern Africa (BOT, SWN, SWS, WCR) compared to REMO (Fig. 13b). In most regions, the results of the coupled model are more shifted towards observations and the ERA-INT driven simulation of REMO. Only a few improvements have been achieved in the simulation of the maximum number of consecutive wet days (CWD) with the coupled model. In ROM, the CWD decreases by -17% over the coastal regions of West Africa (WAS) and by -7 and -14% over southern Africa (SWS, WCR) compared to REMO (Fig. 13c). In these regions, the results of the coupled model are closer to observations and partly also to the ERA-INT driven simulation of REMO.

Major differences and advantages in the use of a coupled model can be seen in the simulation of total annual precipitation on wet days (PRCPTOT). ROM shows a decrease by -27% in total precipitation over the coastal regions of West Africa (WAS), a decrease by -23% over the East African coast (EAC), and over southern Africa (SWN, SWS, WCR) between -15 and -33% (Fig. 13d). The results in ROM are closer to observations in all aforementioned regions, except for EAC, and also closer to the ERA-INT driven simulation of REMO over southern Africa (SWN, SWS, WCR).

The coupled model achieves distinct improvements in simulated extreme precipitation for both R95p and R99p. Compared to REMO, extreme precipitation (R95p, R99p) simulated by ROM decreases by -32 and -30% over the coastal regions of West Africa (WAS) and by -23 and

Fig. 12 Normalized daily precipitation distributions derived from REMO forced with ERA-INT (green), and from REMO (blue) and ROM (red) both forced with MPI-ESM-LR for different African sub-regions from 1981 to 2005 compared to CHIRPS V2.0 (cyan) and ERA5 (purple)



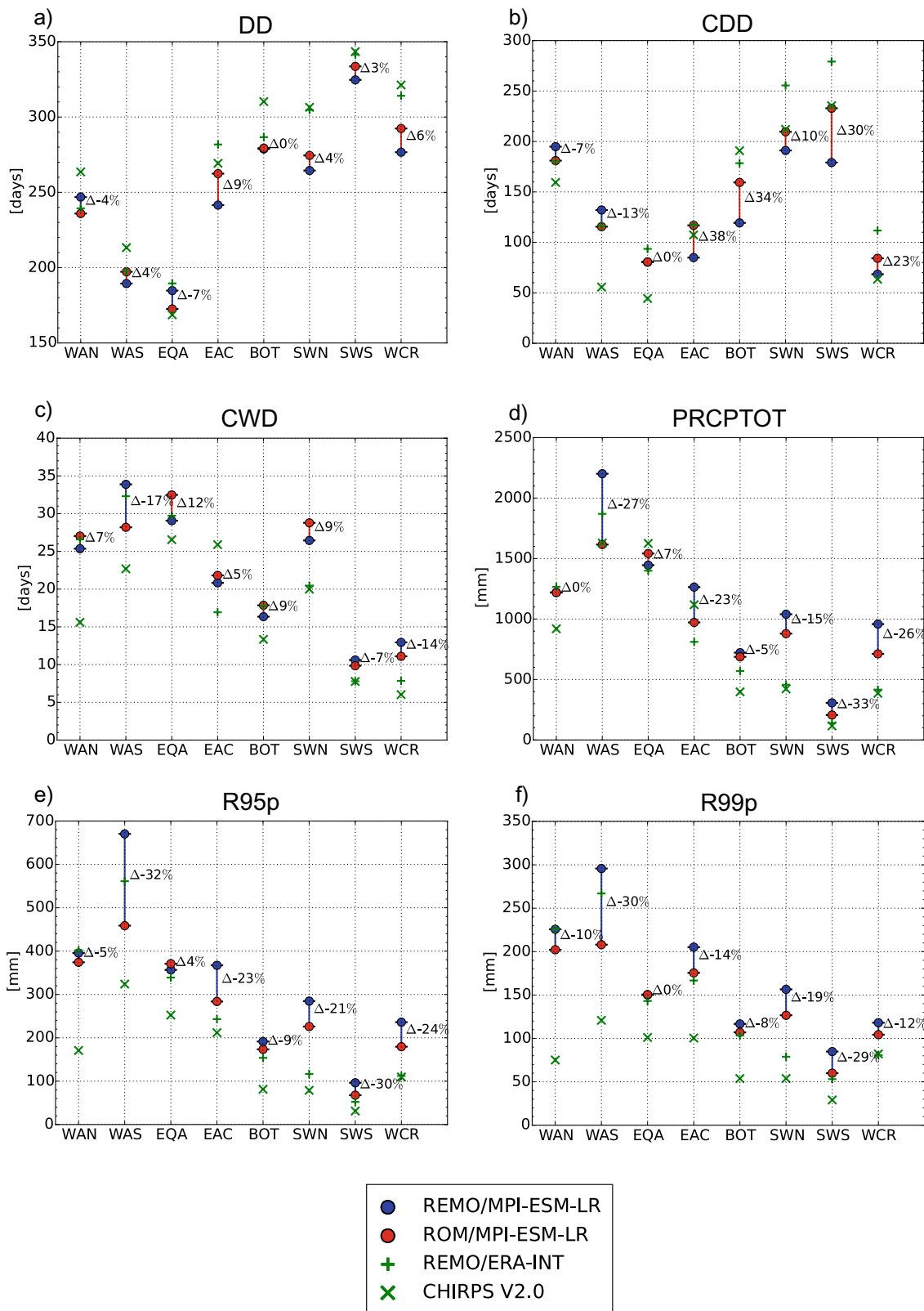


Fig. 13 Evaluation of selected precipitation indices calculated from REMO (blue dots) and ROM (red dots) both forced with MPI-ESM-LR from 1981 to 2005, REMO forced with ERA-INT (green plus)

and CHIRPS V2.0 (green cross) for different African sub-regions. Delta numbers show the relative difference in [%] of ROM minus REMO with respect to REMO

– 14% over the East African coast (EAC), respectively (Fig. 13e, f). Similarly, extreme precipitation in ROM decreases between -8 and -30% over southern Africa (BOT, SWN, SWS, WCR). In all these regions, the results of the coupled model are closer to both observations and the ERA-INT driven simulation of REMO, with the exception of WAS, which is only closer to observations.

Significant effects of atmosphere–ocean coupling are measured over coastal West Africa, where PRCPTOT, R95p and R99p have sharply decreased in ROM. The reason for this is that the ROM model allows the Inter Tropical Convergence Zone (ITCZ) to move further north than the REMO model does. Thus, two lower precipitation maxima in the annual precipitation cycle occur in the coastal regions instead of one large precipitation maximum (Fig. 11b). The increase in DD and CDD over southern Africa in the coupled model can be attributed to a reduced warm SST bias in the Southeast Atlantic. The same is true for the significant decrease in PRCPTOT, R95p and R99p in these regions. Lower simulated SSTs in the Southeast Atlantic lead to a decrease in evaporation over the ocean and, consequently, to a modified vertically integrated moisture transport over southern Africa. In addition, it can be assumed that a complete removal of the SST warm bias in the historical simulation would lead to a further increase of DD and CWD as well as a further reduction of PRCPTOT, R95p and R99p in these regions, as already seen in the reanalysis driven simulation of REMO.

3.4.4 Modification of climate change signals

To investigate the potential changes in precipitation characteristics due to the influence of the regional atmosphere–ocean coupling in a future climate projection, precipitation indices are analyzed in a high emission scenario (RCP8.5) at the end of the century (2070–2099). The decision to use a high emission scenario was made because a high emissions scenario is expected to provide a more significant climate change signal (CCS) than a low emissions scenario. In this way, the maximum impact of atmosphere–ocean coupling on the climate change signals of the indices can be estimated.

ROM and REMO project an increase in the number of annual dry days (DD) with model differences in CCSs between – 6 and +2 days for all sub-regions (Fig. 14a). The largest model difference in CCSs of DD occurs with -6 days in EQA, where the CCS is weaker in ROM than in REMO. Similar to DD, ROM and REMO simulate an increase in the maximum number of consecutive dry days (CDD) for all sub-regions, but with a wider range of model differences in CCSs between – 15 and +49 days (Fig. 14b). Large model differences in CCSs of CDD are simulated with – 15 days for EQA, with +21 days for WCR and with +49 days for SWS. The CCSs of maximum number of consecutive wet

days (CWD) in ROM and REMO decrease for all sub-regions, with model differences in CCSs ranging from – 2 to +1 day (Fig. 14c). In EQA, the CCSs of ROM and REMO are almost the same for EQA and SWS.

For all sub-regions, except EQA, ROM and REMO project a decrease in total annual precipitation on wet days (PRCPTOT) with model differences in CCSs between – 45 and +85 mm (Fig. 14d). In EQA, the CCS of PRCPTOT switches from a slight decrease in REMO to an increase in ROM with a model difference of 80 mm. The largest model differences in CCSs of PRCPTOT occur with +85 mm in WAN and WAS, where the CCSs in ROM are weaker than in REMO.

The CCSs of extreme precipitation (R95p) simulated by ROM and REMO show an increase for the sub-regions WAN, WAS, EQA, EAC and SWN with model differences in CCS between – 22 and +65 mm and a decrease for SWS and WCR with model differences in CCS of – 6 and +11 mm, respectively (Fig. 14e). Only the CCS of R95p in BOT switches from a slight increase in REMO to a decrease in ROM with a model difference of – 21 mm. The largest model difference in CCS of R95p is shown for WAN with +65 mm, where the CCS in ROM is stronger than REMO. For almost all sub-regions, except WCR, CCSs of extreme precipitation (R99p) show an increase in ROM and REMO with model differences between – 36 and +27 mm (Fig. 14f). Only for WCR, ROM and REMO project a decrease in CCS of R99p with a model difference in CCSs of – 12 mm. Moreover, larger model differences in CCS of R99p occur with +27 mm in WAN, where the CCS in ROM is stronger than in REMO, and with – 36 mm in WAS, where the CCSs in ROM is weaker than in REMO.

This experiment shows that the distinct effects of atmospheric-ocean coupling on CCSs are limited to specific regions and indices. The affected regions are West Africa, where the CCS of PRCPTOT (WAN, WAS) and of R95p and R99p (WAN) are distinctly changed, Equatorial Africa (EQA), where the CCS of PRCPTOT is noticeably altered and the outmost southwest of Africa (SWS, WCR), where the CCS of CDD is significantly changed by the coupled model. Considering the observed influence of coupling on CCSs of derived precipitation indices in climate projections, which are commonly generated by uncoupled RCMs (e.g., Nikulin et al. 2018; Weber et al. 2018b; Dosio et al. 2019), CCSs may strengthen or weaken in certain African regions. For instance, an ensemble of uncoupled RCMs projects an increase in extreme precipitation (99th percentile) over coastal regions of West Africa and East Africa with higher global warming levels (Weber et al. 2018b), but our analysis has shown that the CCS of R99p in a high emission scenario would be weaker in a coupled RCM than in an uncoupled one. Similarly,

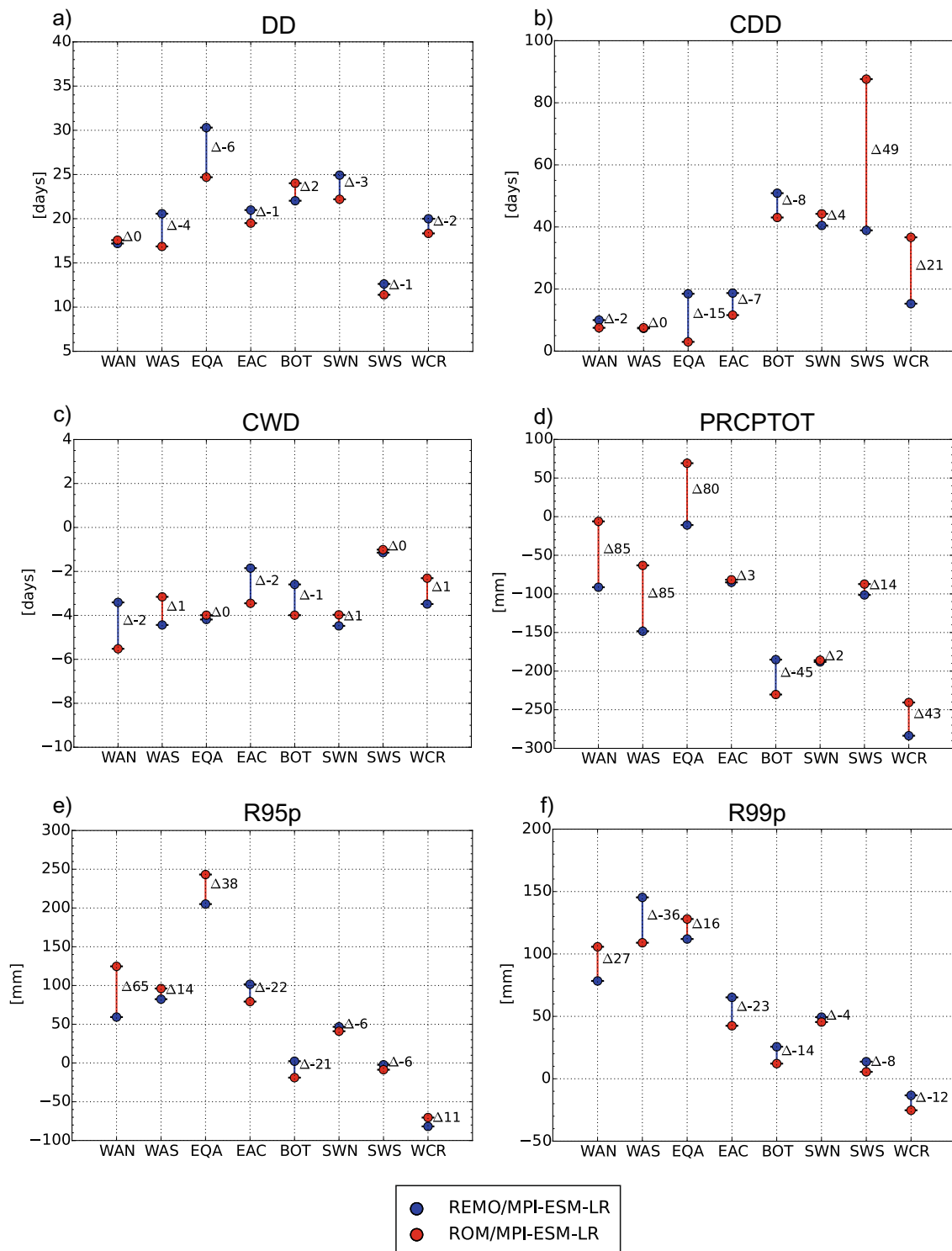


Fig. 14 Climate change signals of selected precipitation indices for different African sub-regions calculated from REMO (blue dots) and ROM (red dots) both forced with MPI-ESM-LR RCP8.5 for 2070–

2099 related to 1971–2000. Delta numbers show the absolute difference of the climate change signal of ROM minus REMO

a decrease in precipitation during the rainy season over WCR is projected with higher global warming (Weber

et al. 2018b), but the CCS of PRCPTOT would be weaker in a high emission scenario simulated by a coupled RCM.

4 Conclusion

Realistic simulations of precipitation characteristics over Africa with regional climate models is a challenge, because precipitation formation over the continent depends on different factors such as sea surface temperature (SST) of the surrounding oceans, evaporation, and moisture transport. This work has analyzed the often neglected impact of the SST bias and the associated changes in moisture transports on precipitation in a regional climate projection over Africa. In detail, we could reveal which African regions and which of the simulated precipitation characteristics are improved by enabling the atmosphere–ocean interaction in a regional climate model.

Decreased biases of the simulated SST in the Southeast Atlantic and Southwest Indian Oceans reduce the precipitation bias over most coastal Sub-Saharan regions and over southern Africa to varying degrees depending on the season. Particularly, annual precipitation cycles over the coastal regions of the Atlantic Ocean are closer to observations, e.g. the bimodal cycle along the coast of Guinea could be reproduced. Furthermore, compared to the uncoupled model, the coupled model simulates small daily precipitation amounts more frequently and large daily precipitation amounts less frequently in the coastal regions of the Atlantic and in the inner parts of West Africa and southern Africa. Simulated daily precipitation amounts in the coupled model are thus more realistic, as a comparison with reanalysis and observation data shows. Distinct changes in precipitation were simulated not only over the African continent. A strong influence of coupling on precipitation was found over small islands located offshore the African coasts, where the precipitation difference between a coupled and an uncoupled model is up to $\pm 100\%$. The coupled model also provides better seasonal precipitation results over islands than the uncoupled model in most cases. This outcome is of crucial importance since climate change analyses for small islands are almost exclusively based on climate projections from uncoupled regional climate models. Furthermore, our results show that precipitation indices relevant for Africa, such as maximum consecutive dry days, total precipitation on wet days, and extreme precipitation, are clearly affected by the coupling and are closer to the observations for the majority of the analyzed sub-regions.

This analysis shows that the climate change signals of precipitation are also influenced by the coupling of atmosphere and ocean in a regional climate model. The climate change signal in the coupled projection is more physically consistent due to the consideration of atmosphere–ocean interactions. It has also been shown that reduced SST biases and the enabled atmosphere–ocean interaction in a regional climate model can modify the

climate change signals of precipitation indices in climate projections. This should be investigated using ensembles of coupled regional climate models to assess whether current climate change information for Africa needs to be revised. The application of model ensembles would also allow the robustness and uncertainty of the CCSs to be estimated, which will provide more confidence in the results. It should be kept in mind that the results obtained in this study also contain some limitations in terms of their validity. The choice of the spatial resolution and the model domain can affect the precipitation results (e.g. Browne and Sylla 2012). In addition, the underlying processes leading to changes in precipitation caused by regional atmosphere–ocean coupling should be the subject of further research, which was outside the scope of this work. Overall, our results suggest that the application of a regionally coupled atmosphere–ocean climate model improves the simulated precipitation characteristics in certain African regions, especially over coastal regions, and should therefore be taken into account for the next-generation of regional climate projections.

Acknowledgements The authors would like to thank the Copernicus Climate Change Service (C3S) Climate Data Store (CDS) for providing the ERA5 reanalysis data set (<https://climate.copernicus.eu/climate-reanalysis>). We acknowledge that this work contains modified Copernicus Climate Change Service Information and neither the European Commission nor ECMWF is responsible for any use that may be made of the Copernicus information or data it contains. In addition, we would like to thank the European Centre for Medium-Range Weather Forecasts (ECMWF) for providing the ERA-Interim reanalysis data set (<https://www.ecmwf.int/en/forecasts/datasets/reanalysis-datasets/era-interim>). We acknowledge the Global Precipitation Climatology Centre (GPCC) (<https://www.dwd.de/EN/ourservices/gpcc/gpcc.html>), the Climate Hazards Center of the University of California (<https://www.chc.ucsb.edu/data/chirps>) and the Climatic Research Unit of the University of East Anglia (<https://sites.uea.ac.uk/cru/>) for the provision of their observational precipitation data sets. NOAA High Resolution SST data was provided by the NOAA/OAR/ESRL PSL, Boulder, Colorado, USA, from their web site at <https://downloads.psl.noaa.gov/Datasets/noaa.oisst.v2.highres/>. The model simulations were performed at the German Climate Computing Center (Deutsches Klimarechenzentrum, DKRZ) in Hamburg. Dmitry Sein was supported in the framework of the state assignment of the Ministry of Science and Higher Education of Russia (№ FMWE-2021-0014). Finally, the authors would like to thank the anonymous reviewers and the colleagues of the Climate Service Center Germany (GERICS) for their constructive support.

Author contributions Conceptualization: TW, WC, DS, DJ. Methodology: DS, WC. Formal analysis and investigation: TW, WC, DS. Visualization: TW, DS. Writing—original draft preparation: TW, DS. Writing—review and editing: WC, DJ. Resources: DJ.

Funding Open Access funding enabled and organized by Projekt DEAL.

Availability of data and material (data transparency) Model forcing data and observational data are freely available, model output data is not public accessible.

Code availability (software application or custom code) The model codes of ROM and REMO can be requested from the Alfred Wegener Institute for Polar and Marine Research and the Climate Service Center Germany (GERICS). Scripts for data processing are stored in an internal GitLab, software used are Bash scripts, CDO and Python.

Declarations

Conflict of interest There are no conflicts of interest or competing interests.

Open Access This article is licensed under a Creative Commons Attribution 4.0 International License, which permits use, sharing, adaptation, distribution and reproduction in any medium or format, as long as you give appropriate credit to the original author(s) and the source, provide a link to the Creative Commons licence, and indicate if changes were made. The images or other third party material in this article are included in the article's Creative Commons licence, unless indicated otherwise in a credit line to the material. If material is not included in the article's Creative Commons licence and your intended use is not permitted by statutory regulation or exceeds the permitted use, you will need to obtain permission directly from the copyright holder. To view a copy of this licence, visit <http://creativecommons.org/licenses/by/4.0/>.

References

- Akinsanola AA, Ogunjobi KO, Vincent VO, Adefisan EA, Omotosho JA, Sanogo S (2017) Comparison of five gridded precipitation products at climatological scales over West Africa. *Meteorol Atmos Phys*. <https://doi.org/10.1007/s00703-016-0493-6>
- Bougeault P (1983) A non-reflective upper boundary condition for limited-height hydrostatic models. *Mon Weather Rev* 111:420–429. [https://doi.org/10.1175/1520-0493\(1983\)111%3c0420:ANRUBC%3e2.0.CO;2](https://doi.org/10.1175/1520-0493(1983)111%3c0420:ANRUBC%3e2.0.CO;2)
- Browne NAK, Sylla MB (2012) Regional climate model sensitivity to domain size for the simulation of the West African summer monsoon rainfall. *Int J Geophys*. <https://doi.org/10.1155/2012/625831>
- Cabos W, Sein DV, Pinto JG et al (2017) The South Atlantic Anticyclone as a key player for the representation of the tropical Atlantic climate in coupled climate models. *Clim Dyn* 48:4051–4069. <https://doi.org/10.1007/s00382-016-3319-9>
- Cabos W, De la Vara A, Álvarez FJ et al (2020) Impact of ocean-atmosphere coupling on regional climate: the Iberian Peninsula case. *Clim Dyn* 54:4441–4467. <https://doi.org/10.1007/s00382-020-05238-x>
- Davies HC (1976) A lateral boundary formulation for multi-level prediction models. *Q J R Meteorol Soc* 102:405–418
- De la Vara A, Cabos W, Sein DV et al (2020) On the impact of atmospheric vs oceanic resolutions on the representation of the sea surface temperature in the South Eastern Tropical Atlantic. *Clim Dyn* 54:4733–4757. <https://doi.org/10.1007/s00382-020-05256-9>
- Dee DP, Uppala SM, Simmons AJ et al (2011) The ERA-Interim reanalysis: configuration and performance of the data assimilation system. *Q J R Meteorol Soc* 137:553–597. <https://doi.org/10.1002/qj.828>
- Déqué M, Somot S, Sanchez-Gomez E et al (2012) The spread amongst ENSEMBLES regional scenarios: regional climate models, driving general circulation models and interannual variability. *Clim Dyn* 38:951–964. <https://doi.org/10.1007/s00382-011-1053-x>
- Dosio A, Panitz HJ, Schubert-Frisius M et al (2015) Dynamical downscaling of CMIP5 global circulation models over CORDEX-Africa with COSMO-CLM: evaluation over the present climate and analysis of the added value. *Clim Dyn* 44:2637–2661. <https://doi.org/10.1007/s00382-014-2262-x>
- Dosio A, Jones RG, Jack C et al (2019) What can we know about future precipitation in Africa? Robustness, significance and added value of projections from a large ensemble of regional climate models. *Clim Dyn* 53:5833–5858. <https://doi.org/10.1007/s00382-019-04900-3>
- Eichhorn A, Bader J (2017) Impact of tropical Atlantic sea-surface temperature biases on the simulated atmospheric circulation and precipitation over the Atlantic region: an ECHAM6 model study. *Clim Dyn* 49:2061–2075. <https://doi.org/10.1007/s00382-016-3415-x>
- Exarchou E, Prodhomme C, Brodeau L et al (2018) Origin of the warm eastern tropical Atlantic SST bias in a climate model. *Clim Dyn* 51:1819–1840. <https://doi.org/10.1007/s00382-017-3984-3>
- Funk CC, Peterson PJ, Landsfeld MF, Pedreros DH, Verdin JP, Rowland JD, Romero BE, Husak GJ, Michaelsen JC, Verdin AP (2014) A quasi-global precipitation time series for drought monitoring: U.S. Geol Surv Data Ser 832:4. <https://doi.org/10.3133/ds832>
- Funk C, Peterson P, Landsfeld M et al (2015) The climate hazards infrared precipitation with stations—a new environmental record for monitoring extremes. *Sci Data* 2:150066. <https://doi.org/10.1038/sdata.2015.66>
- Găinușă-Bogdan A, Hourdin F, Traore AK, Braconnot P (2018) Omens of coupled model biases in the CMIP5 AMIP simulations. *Clim Dyn* 51:1–15. <https://doi.org/10.1007/s00382-017-4057-3>
- Haensler A, Hagemann S, Jacob D (2011) The role of the simulation setup in a long-term high-resolution climate change projection for the southern African region. *Theor Appl Climatol* 106:153–169. <https://doi.org/10.1007/s00704-011-0420-1>
- Hagemann S, Dümenil Gates L (2001) Validation of the hydrological cycle of ECMWF and NCEP reanalyses using the MPI hydrological discharge model. *J Geophys Res* 106:1503–1510
- Harris I, Osborn TJ, Jones P, Lister D (2020) Version 4 of the CRU TS monthly high-resolution gridded multivariate climate dataset. *Sci Data* 7:109. <https://doi.org/10.1038/s41597-020-0453-3>
- Hernández-Díaz L, Laprise R, Nikiéma O, Winger K (2017) 3-Step dynamical downscaling with empirical correction of sea-surface conditions: application to a CORDEX Africa simulation. *Clim Dyn* 48:2215–2233. <https://doi.org/10.1007/s00382-016-3201-9>
- Hersbach H, Bell B, Berrisford P et al (2018) ERA5 hourly data on single levels from 1979 to present. Copernicus Climate Change Service (C3S) Climate Data Store (CDS). <https://doi.org/10.24381/cds.adbb2d47>. Accessed 14 May 2019
- Hersbach H, Bell B, Berrisford P et al (2020) The ERA5 global reanalysis. *Q J R Meteorol Soc* 146:1999–2049. <https://doi.org/10.1002/qj.3803>
- Hoffmann P, Katzfey JJ, McGregor JL, Thatcher M (2016) Bias and variance correction of sea surface temperatures used for dynamical downscaling. *J Geophys Res* 121:12877–12890. <https://doi.org/10.1002/2016JD025383>
- Huang B, Liu C, Banzon V, Freeman E, Graham G, Hankins B, Smith T, Zhang H-M (2021) Improvements of the Daily Optimum Interpolation Sea Surface Temperature (DOISST) Version 2.1. *J Clim* 34:2923–2939. <https://doi.org/10.1175/JCLI-D-20-0166.1>
- Jacob D (2001) The role of water vapour in the atmosphere. A short overview from a climate modeller's point of view. *Phys Chem Earth A* 26:523–527
- Jacob D, Elizalde A, Haensler A et al (2012) Assessing the transferability of the regional climate model REMO to different coordinated regional climate downscaling experiment (CORDEX)

- regions. *Atmosphere (basel)* 3:181–199. <https://doi.org/10.3390/atmos3010181>
- Jungclaus JH, Fischer N, Haak H, Lohmann K, Marotzke J, Matei D, Mikolajewicz U, Notz D, von Storch JS (2013) Characteristics of the ocean simulations in MPIOM, the ocean component of the MPI-Earth system model. *J Adv Model Earth Syst* 5:422–446. <https://doi.org/10.1002/jame.20023>
- Klemp JB, Duran DR (1983) An upper boundary condition permitting internal gravity wave radiation in numerical mesoscale models. *Mon Weather Rev* 11:430–444. [https://doi.org/10.1175/1520-0493\(1983\)111%3c0430:AUBCP1%3e2.0.CO;2](https://doi.org/10.1175/1520-0493(1983)111%3c0430:AUBCP1%3e2.0.CO;2)
- Kotlarski S, Keuler K, Christensen OB et al (2014) Regional climate modeling on European scales: a joint standard evaluation of the EURO-CORDEX RCM ensemble. *Geosci Model Dev* 7:1297–1333. <https://doi.org/10.5194/gmd-7-1297-2014>
- Lengaigne M, Neetu S, Samson G et al (2019) Influence of air–sea coupling on Indian Ocean tropical cyclones. *Clim Dyn* 52:577–598. <https://doi.org/10.1007/s00382-018-4152-0>
- Lima DCA, Soares PMM, Semedo A et al (2019) How will a warming climate affect the Benguela Coastal low-level wind jet? *J Geophys Res Atmos* 124:5010–5028. <https://doi.org/10.1029/2018JD029574>
- Lutz K, Jacobeit J, Rathmann J (2015) Atlantic warm and cold water events and impact on African west coast precipitation. *Int J Climatol* 35:128–141. <https://doi.org/10.1002/joc.3969>
- Majewski D (1991) The Europa model of the Deutscher Wetterdienst. In: Seminar Proceedings ECMWF, vol. 2, ECMWF, Reading, U. K., pp 147–191
- Marsland SJ, Haak H, Jungclaus JH, Latif M, Roeske F (2003) The Max-Planck-Institute global ocean/sea ice model with orthogonal curvilinear coordinates. *Ocean Model* 5(2):91–127. [https://doi.org/10.1016/S1463-5003\(02\)00015-X](https://doi.org/10.1016/S1463-5003(02)00015-X)
- Niang I, Ruppel OC, Abdrabo MA, Essel A, Lennard C, Padgham J, Urquhart P (2014) Africa. In: *Climate Change 2014: Impacts, Adaptation, and Vulnerability. Part B: Regional Aspects. Contribution of Working Group II to the Fifth Assessment Report of the Intergovernmental Panel on Climate Change* [Barros VR, Field CB, Dokken DJ, Mastrandrea MD, Mach KJ, Bilir TE, Chatterjee M, Ebi KL, Estrada YO, Genova RC, Girma B, Kissel ES, Levy AN, MacCracken S, Mastrandrea PR, White LL (eds.)]. Cambridge University Press, Cambridge, United Kingdom and New York, NY, USA, pp 1199–1265
- Nikulin G, Lennard C, Dosio A et al (2018) The effects of 1.5 and 2 degrees of global warming on Africa in the CORDEX ensemble. *Environ Res Lett*. <https://doi.org/10.1088/1748-9326/aab1b1>
- Paxian A, Sein D, Panitz H-J et al (2016) Bias reduction in decadal predictions of West African monsoon rainfall using regional climate models. *J Geophys Res Atmos* 121:1715–1735. <https://doi.org/10.1002/2015JD024143>
- Ratnam JV, Behera SK, Ratna SB et al (2013) Dynamical Downscaling of Austral Summer Climate Forecasts over Southern Africa Using a Regional Coupled Model. *J Clim* 26:6015–6032. <https://doi.org/10.1175/JCLI-D-12-00645.1>
- Ratnam JV, Morioka Y, Behera SK, Yamagata T (2015) A model study of regional air–sea interaction in the austral summer precipitation over southern Africa. *J Geophys Res*. <https://doi.org/10.1002/2014JD022154>
- Remedio AR, Teichmann C, Buntmeyer L, Sieck K, Weber T, Rechid D et al (2019) Evaluation of new CORDEX simulations using an updated Köppen-Trewartha climate classification. *Atmosphere* 10(11):726. <https://doi.org/10.3390/atmos10110726>
- Reynolds RW, Smith TM, Liu C, Chelton DB, Casey KS, Schlax MG (2007) Daily high-resolution-blended analyses for sea surface temperature. *J Clim* 20:5473–5496. <https://doi.org/10.1175/2007JCLI1824.1>
- Riahi K, Rao S, Krey V et al (2011) RCP 8.5—a scenario of comparatively high greenhouse gas emissions. *Clim Change* 109:33. <https://doi.org/10.1007/s10584-011-0149-y>
- Roeckner E, Arpe K, Bengtsson L, Christoph M, Claussen M, Dümenil L, Esch M, Giorgetta M, Schlese U, Schulzweida U (1996) The atmospheric general circulation model ECHAM-4: Model description and simulation of present day climate. Report No. 218:90. Max Planck Institute for Meteorology, Hamburg
- Roeckner E, et al (2003) The atmospheric general circulation model ECHAM 5. PART I: Model description Rep. 349, MPI für Meteorol, Hamburg, Germany
- Schneider U, Becker A, Finger P, Rustemeier E, Ziese M (2020) GPCP Full Data Monthly Product Version 2020 at 0.25°: Monthly Land-Surface Precipitation from Rain-Gauges built on GTS-based and Historical Data. https://doi.org/10.5676/DWD_GPCP/FD_M_V2020_025
- Sein DV, Koldunov NV, Pinto JG, Cabos W (2014) Sensitivity of simulated regional Arctic climate to the choice of coupled model domain. *Tellus A* 66:23966. <https://doi.org/10.3402/tellusa.v66.23966>
- Sein DV, Mikolajewicz U, Gröger M, Fast I, Cabos W, Pinto JG, Hagemann S, Semmler T, Izquierdo A, Jacob D (2015) Regionally coupled atmosphere–ocean–sea ice–marine biogeochemistry model ROM: 1. Description and validation. *J Adv Model Earth Syst* 7:268–304. <https://doi.org/10.1002/2014MS000357>
- Soares PMM, Cardoso RM (2018) A simple method to assess the added value using high-resolution climate distributions: application to the EURO-CORDEX daily precipitation. *Int J Climatol* 38:1484–1498. <https://doi.org/10.1002/joc.5261>
- Soares PMM, Lima DCA, Semedo A et al (2019) Assessing the climate change impact on the North African offshore surface wind and coastal low-level jet using coupled and uncoupled regional climate simulations. *Clim Dyn* 52:7111–7132. <https://doi.org/10.1007/s00382-018-4565-9>
- Soto-Navarro J, Jordá G, Amores A et al (2020) Evolution of Mediterranean Sea water properties under climate change scenarios in the Med-CORDEX ensemble. *Clim Dyn* 54:2135–2165. <https://doi.org/10.1007/s00382-019-05105-4>
- Stevens B, Giorgetta M, Esch M, Mauritsen T, Crueger T, Rast S, Salzmann M, Schmidt H, Bader J, Block K, Brokopf R, Fast I, Kinne S, Kornbluh L, Lohmann U, Pincus R, Reichler T, Roeckner E (2013) The atmospheric component of the MPI-M earth system model: ECHAM6. *J Adv Model Earth Syst* 5:46–172. <https://doi.org/10.1002/jame.20015>
- Sylla MB, Giorgi F, Coppola E, Mariotti L (2013) Uncertainties in daily rainfall over Africa: assessment of gridded observation products and evaluation of a regional climate model simulation. *Int J Climatol* 33:1805–1817. <https://doi.org/10.1002/joc.3551>
- Teichmann C, Jacob D, Remedio AR et al (2021) Assessing mean climate change signals in the global CORDEX-CORE ensemble. *Clim Dyn* 57:1269–1292. <https://doi.org/10.1007/s00382-020-05494-x>
- Toniazzo T, Woolnough S (2014) Development of warm SST errors in the southern tropical Atlantic in CMIP5 decadal hindcasts. *Clim Dyn* 43:2889. <https://doi.org/10.1007/s00382-013-1691-2>
- Valcke S, Caubel A, Declat D, Terray L (2003) OASIS3 Ocean Atmosphere Sea Ice Soil User's Guide, Tech. Rep. TR/CMGC/03–69, CERFACS, Toulouse, France.
- Van der Ent RJ, Savenije HHG (2013) Oceanic sources of continental precipitation and the correlation with sea surface temperature. *Water Resour Res* 49:3993–4004. <https://doi.org/10.1002/wrcr.20296>
- Washington R, Preston A (2006) Extreme wet years over southern Africa: role of Indian Ocean sea surface temperatures. *J Geophys Res Atmos* 111:1–15. <https://doi.org/10.1029/2005JD006724>

- Weber T, Haensler A, Jacob D (2018a) Sensitivity of the atmospheric water cycle to corrections of the sea surface temperature bias over southern Africa in a regional climate model. *Clim Dyn* 51:2841–2855. <https://doi.org/10.1007/s00382-017-4052-8>
- Weber T, Haensler A, Rechid D et al (2018b) Analysing regional climate change in Africa in a 1.5, 2 and 3°C global warming world. <https://doi.org/10.1002/2017EF000714>
- Xu Z, Chang P, Richter I et al (2014) Diagnosing southeast tropical Atlantic SST and ocean circulation biases in the CMIP5 ensemble. *Clim Dyn* 43:3123–3145. <https://doi.org/10.1007/s00382-014-2247-9>

Publisher's Note Springer Nature remains neutral with regard to jurisdictional claims in published maps and institutional affiliations.